Development and Initial Results of an Industrial Prototype Vaporizing Foil Actuated Welding Device

Undergraduate Research Thesis

Presented in partial fulfillment of the requirements for graduation with Honors Research Distinction in Materials Science and Engineering in the undergraduate college of The Ohio State University

By

Yu Mao

Undergraduate Program in Materials Science and Engineering

The Ohio State University

2016

Thesis Committee:

Glenn Daehn, Advisor

Copyright by

Yu Mao

2016

Abstract

Vaporizing Foil Actuated Welding (VFAW) is a novel collision welding technique for metal joining of moderate to small length scales developed at the Ohio State University. A flyer is accelerated towards a target.by a high-pressure pulse generated by electrically driven vaporization of an aluminum foil and then produces a collision welding. Compared with conventional fusion-based welding, it allows joining of dissimilar metals with large separate melting points and produces little to no heat-affected zones with a much higher energy-efficiency. Currently, one big constraint on industrial adoption of VFAW is the complexity and inefficiency of required manual setup before each weld. The goal of the project is to further develop the VFAW technique and improve its Technology Readiness Level by constructing an effective, automated, industrial-level prototype system and to explore the effects of different input parameters on VFAW efficiency. The construction process included design and fabrication of components, system integration, and program setup. A VFAW system with charging capability of 3.0 kJ and a discharge frequency of 35.7 kHz was constructed and achieved continuous spot welds at a rate of one minute per weld, which is 20 times faster than before. The new device was able to weld similar aluminum alloys and steels at energy levels below 2 kJ. Spot welding of Al 5052 to JSC590R was researched using the system. The energy deposition on the 0.0762 mm-thick aluminum foil at input energy of 2.6 kJ is obtained as 2347 J. Parameters of VFAW including input energy, foil geometry, and preformation geometry were explored. The collision velocity of one parameter combination was

determined as 753 m/s. It is proved that no heat-affected zone was created during welding according to the micro-hardness test.

Dedication

Dedicated to my mother and father

Acknowledgments

I would like to thank Prof. Glenn Daehn for his approval of the project, who gave me the valuable opportunity to be a researcher in the laboratory. I would thank Mr. Geoffrey Taber for his work on the construction of the capacitor bank and more importantly, his guidance and encouragement to me, who impressed me by his great passion in life. I would thank Dr. Anupam Vivek for his guidance and support on the research, who acted as a model of a professional engineer for me. I would thank Brain Thurston for his work on the weld head, his work of producing the dies, and his help with welds and shear tensile tests. I would thank Dr. Yongbo Wan for his help with system integration and work on the circuit diagram.

Additionally, the work on this project has been performed with the support of an accelerator award from the Ohio State University, a TVSF award from Ohio Development Services Agency and a grant from the United States Department of Energy.

Vita

September 2007 – July 2010 .....Zibo Experimental High School

September 2010 – November 2012 .....Shanghai Jiao Tong University

January 2013 – present ……. The Ohio State University

Field of Study

Major Field: Materials Science and Engineering

Table of Contents

List of Tables

List of Figures

Chapter 1: Overview

1.1 Motivation

Conventional fusion-based welding of metals with widely disparate melting temperature, such as aluminum and steel, is very difficult. Fusion-based welding also impairs mechanical properties of welded components by creating heat-affected zones. These processes are also very energy intensive and can take up to 50 kJ of electrical energy for a single resistance spot weld for example (Briskham et al. 2006). Vaporizing Foil Actuator Welding (VFAW), a novel welding technique developed by Impulse Manufacturing Laboratory, OSU, utilizes a high-pressure pulse generated by the vaporization of aluminum foils to create impact welds. It is a solid-state welding method allowing joining of dissimilar metals with producing little to no heat-affected zones and has much lower input energy than conventional welding. As a promising alternative joining method in comparison to fasteners and rivets, this technology enables the creation of multi-material lightweight structures for large industries such as automotive and aerospace in the future.

1.2 Introduction

VFAW is a small scale collision welding technique for millimeter-thick sheets. Vivek et al. (2013) firstly introduced it and successfully created welding couples of copper-

titanium, copper-steel, aluminum-copper, aluminum-magnesium, and titanium-steel. VFAW makes use of shock waves from plasma generated by electrically driven vaporizing aluminum foils to launch a flyer toward a stationary target. Then a collision between the flyer and the target at appropriate angle and velocity creates the impact weld. A schematic of VFAW (Vivek et al., 2013) is shown in Fig.1.

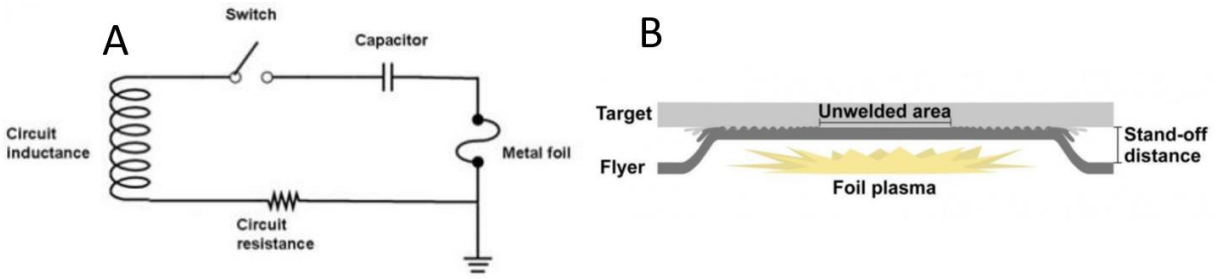

Fig. 1. Schematic of electrically driven vaporizing metallic foils (A) and schematic of a collision welding process (B)

1.2.1 Electrically driven vaporizing metallic foils

When a large pulsed current in the order of tens of kilo-amperes discharges through a thin metallic conductor in very short time in the order of several microseconds, a fast electrical explosion of the conductor will drive the foil into states of gas and aggregated plasma, producing shock waves, electrictro magnetic waves, and heat. The process is also referred to as electrically driven rapidly vaporizing foils. The technique was firstly developed in 1960's. Keller, Penning (1962) and Guenther et al. (1962) successfully used electrically exploding metal foils to accelerate thin plates of dielectric material to

velocities of 4-5 km/s. Research and applications on electrically driven vaporizing metallic foils have developed in the areas of materials science and shock wave physics. Kotov, Samatov (1999) and Suzuki et al. (2001) produced nanosized ceramic powders by the exploding wire method. Chau et al. (1980) presented that electrically driven vaporizing metallic foils is a viable and versatile tool for creating planar shock waves, which is capable of driving thin flyer to velocities in the range 1-20 km/s and generating shock pressure in excess of 1 TPa (Weingart, 1980).

According to Wang et al. (2011), the electrically driven vaporizing metallic conductors is a magnetohydrodynamic process going through initial stages, including the stage of heating, the stage of melting and the heating stage of liquid metal before vaporizing, and second stages, including the stage of vaporizing and the following plasma forming. The vaporizing of liquid metal greatly increases its resistance and results in fast increase of the induction voltage between the foil, causing the vapor breakdown into plasma and then decrease of resistance (Wang et al., 2011). According to Hahn et al. (2016), if the deposited electrical energy E_d until the burst of the foil at time t_b exceeds the theoretical sublimation energy of the foil before vaporizing, the impulse pressure will result from the expanding vapor and plasma driven by the deposited energy triggered at t_b by the heat-induced breakdown of the dynamic equilibrium between increasing vapor pressure and constraining Lorentz force around the vapor. The breakdown is an instantaneous process indicated by the peak in voltage. Typical waveforms of discharging current and voltage is shown as Fig. 2 (Wang et al. 2011). Chau et al. (1980) showed that the aluminum foil is the best material for electrical vaporization to drive a high velocity flyer. Based on

Gurney energy model applied on electrical driven explosion of metallic conductors by Tucker and Stanton (1975) and work of Osher et al. (1989), Chau et al. (1980), Cho et al. (2004), Grigoriev and Pavlenko (2009), Vivek et al. (2014b) created a viable simple analytical model for predicting the flyer velocity V by using input parameters of deposited electrical energy before its burst, E_d, sublimation energy of the foil, E_s, the ratio of mass of the flyer and foil, and the mass of the flyer, M_f, as

$$V = k * \left(\frac{E_d - E_s}{Mf}\right)^{\frac{1}{2}} \quad \text{Eq. 1}$$

where k is a constant depending on the ratio of mass of the flyer and foil, and E_d can be obtained as the electrical power integral overtime

$$E_d = \int_0^{t_b} v(t) * i(t) dt \quad \text{Eq .2}$$

where v(t) is the voltage and i(t) is the current. Also, Grigoriev and Pavlenko (2009) hypothesized a linear increasing relationship between the pressure pulse amplitude and the ratio of E_d and the heat of vaporization of the foil.

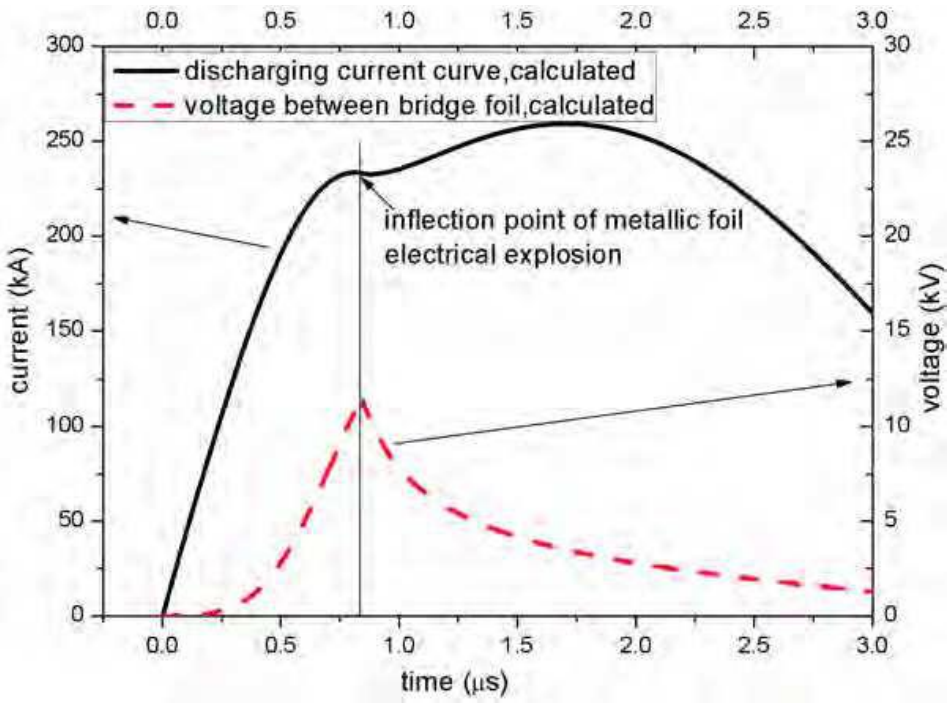

Fig. 2. Typical waveforms of current and voltage during the electrical explosion of a metallic conductor (Wang et al., 2011)

1.2.2 Collision welding technique

A collision between two clean pieces of metal at an appropriate velocity and angle creates weld. During impact, the impact pressures can be up to several gigapascals (Mori et al. 2013), resulting in a jet that removes the surface oxides and contaminants, and then clean metal surfaces are contacted. When atoms of two metal pieces are close enough without any barrier, metallic bonds are created, which is actually a weld. The technique does not involve the melting of the metal, so metals with widely separate melting points can also be collision welded. Using the technique, Explosive Welding (EXW), which obtains high velocity through large quantities of chemical explosives, was first developed to join large

scale dissimilar metals since the 1950's. Magnetic Pulse Welding (MPW) is the other common collision welding technique useful for smaller scale weld on the order of centimeters, making use of the repulsion of Lorentz force to accelerate the flyer. Watanabe et al. (2006) and Okagawa and Aizawa (2004) produced welds of thin aluminum sheets with nickel, iron and copper using MPW. However, EXW is most suited for welding at length scales on the order of meters and is very energy intensive. MPW is limited by the longevity of the actuator and influenced by the resistivity of the flyer plate material (Golovashchenko 2013). In comparison, VFAW is a novel collision welding technique useful for small scale metals without issues of coil longevity and resistivity of the flyer. Moreover, VFAW can provide much higher impact velocity than MPW at same charging energy and standoff (Hahn et al. 2016).

For an ideal collision weld, weld seam propagates through the jet in the form of wavy interface morphology (Vivek, et al., 2014a). Mechanism of creation of the wavy pattern is still under discussion. A Kelvin-Helmholtz hydrodynamic instability mechanism was proposed by Ben-Artzy et al. (2010) based on the interaction of reflected shock waves at the collision point. A schematic of creation of welding by collision is shown as Fig.1(b). Kore et al. (2009) proved that welds with wavy interface morphology do not go through melting and solidification stage and therefore maintains good mechanical properties of the base meals. The weldability domain, so called a welding window, consists of two important parameters, collision velocity and impact angle. Successful collision welds can be created at impact velocities in the range of 150-1500 m/s and impact angles between 5° and 20° (Vivek et al., 2013). Vivek et al. (2014a) presented welding windows of cp Ti-

Cu 110 VFAW joints. In VFAW, collision angle is determined by standoff gap and pre-deformation of the target and affected by foil geometry as well as impact velocity.

1.2.3 Al-Fe intermetallic compound

Instead of a wavy-pattern weld seam without going through melting and solidification stage, an imperfect collision will lead to transformation of kinetic energy to heat energy, causing high-temperature heating, melting and mixing of Al and Fe in contact with each other. Intermetallic Compound (IMC) layer of Al and Fe will be created. Al-rich IMCs are hard and brittle and is therefore one of main issues of welding aluminum to steel (Ozaki and Kutsuna, 2012). Fe-Al phase diagram (Massalski, et al., 1986) is shown as Fig. 3.

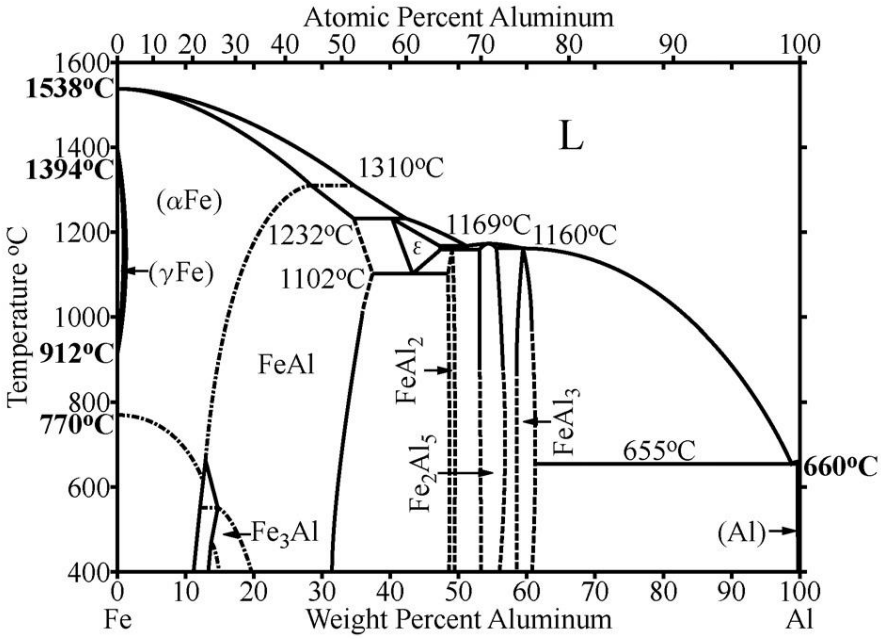

Fig. 3: Fe-Al equilibrium phase diagram

1.3 Objectives

The objective of the project was to further develop the VFAW technique and improve its Technology Readiness Level by constructing an effective, automated, industrial-level prototype system and to explore the effects of different input parameters on VFAW efficiency. The system can be programmed to release an accurate amount of energy from numerical input and supports automatic continuous shots at the rate of 1 shot per minute by user-friendly and safe interface control. The system was expected to be more capable of depositing energy into aluminum foils having active mass optimized for spot welding geometry than the two current capacitor banks. Measurements of flyer velocity by a Photonic Doppler Velocimetry (PDV) system and short current rise time were performed to characterize the system. Spot welding of aluminum 5052-JSR590R steel was researched using the system. Parameters of VFAW including input energy, the geometry of aluminum foils, and the geometry of pre-deformed standoff were explored. Lap joint shear test of welds, optical microscopic characterization on weld cross-section, and micro-hardness tests on the weld were performed to analyze welds. In order to develop VFAW technique, the project had two goals: optimization of the electrically rapid vaporizing foils driven pulse power supply for a faster current-rise time and optimization of the collision welding by exploring the other parameters influencing join strength.

Chapter 2: Approaches and Methodologies

2.1 Construction of an integrated electro-mechanical VFAW system

2.1.1 The RLC system capable of higher flyer velocity

According to Eq. 1, using the same foil and flyer, the velocity of the flyer increases with E_d. Cho et al. (2004) proposed that E_d increases as increased input energy, faster current-rise, and increased atmospheric pressure. Vivek et al. (2014b) proved that using the same capacitor bank, in the range of operation voltage of VFAW, E_d increases as the increase of input energy; however, the increase is not linear and results in a diminishing return. Likewise, increasing atmospheric pressure may not be valid for VFAW because it involves inevitable increase of air dragging of the flyer and it requires extra device for pressure control. As a result, increase of current-rise was considered to be a viable approach to increase E_d, and therefore to increase the flyer velocity. At the same energy, the current-rise can be increased by increasing discharging voltage and decreasing the capacitance. Consequently, the system could be optimized by using lower capacitance. Four capacitors of 13 μF were connected in parallel to obtain a total capacitance of 52 μF.

2.1.2 The mechanical switch

A reliable switch is considered a vital component of the capacitor bank because the operation voltage can be up to more than 10 kV with current of several tens of kiloamperes. A two-electrode switch with one fixed electrode and moveable electrode driven by pneumatic cylinder through a valve controlled by electrical manifold was conceived. Copper-Tungsten alloy was selected by reason of its good heat-resistance, good ablation-resistance, electrical conductivity, and good machinability. Compressed air flows through the controlled electrical manifold to the pneumatic cylinder.

2.1.3 Control of the system

A Programmable Logic Controller (PLC) with a touch screen human-machine interface is used to control the operation of the capacitors by subsystems, and peripheral components, including a LED detector, a high voltage power supply, a high power resistor, an air gas cylinder, the switch, and electrical manifold modules. The LED detector detects the status and motion of the switch and sends them to PLC. The high voltage power supply is controlled by PLC to charge the capacitors to required voltage. It also monitors the voltage of the capacitor and gives the value as well as the signal of charge complete to PLC. The manifold modules are controlled by PLC to control the motion of the switch and action of the vent in the switch with the air gas cylinder as the source of mechanical force. The motion of the switch can fire the bank and discharge the capacitors. The high power resistor is controlled by the PLC through a relay to dispose the charge in the capacitors. The HMI panel inputs the numerical value of required discharge energy to PLC, gives order of action to PLC, and shows the status of system output from PLC.

Analog modules are used for transformation between digital and analog signals. The signal flows are shown as Table 1. Working cycle of the system in the mode of manual single shot is shown as Fig. 4.

Table 1. Signal flows of the system

	Signal	Device	Signal type
Signals input to PLC	Numerical input of required energy	HMI panel → PLC	Digital
	Order of actions	HMI panel→ PLC	Digital
	Status of the switch	LED detector→ PLC	Digital
	Real-time capacitor voltage	High power supply→ Analog input module → PLC	Analog → Digital
	Charge complete	High power supply → PLC	Digital
Signals output from PLC	Required charge voltage	PLC → Analog output module → High voltage power supply	Digital → Analog
	Motion of the switch	PLC → Electrical manifold modules → Switch	Digital → Mechanical motion
	Control of the safety contactor	PLC → Safety contactor → high power dump resistor	Digital → Mechanical motion

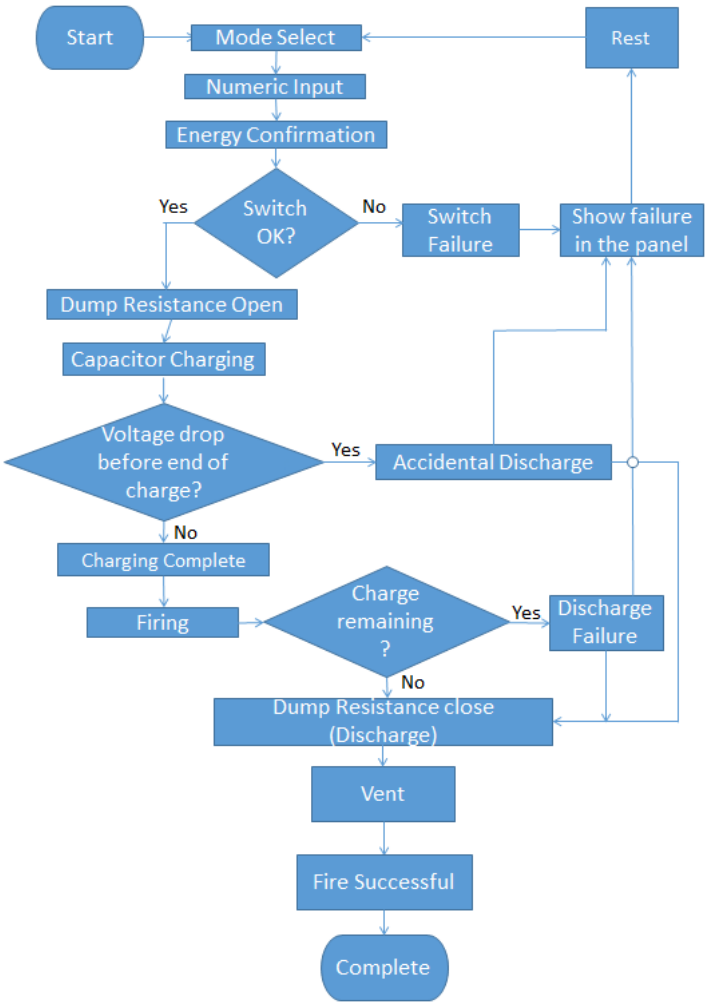

Fig. 4. Working cycle of the system in the mode of manual single shot

2.1.3 System characterization: measurement of current-rise time and energy deposition

The current-rise time is an important intrinsic parameter of a capacitor bank describing its discharging speed, which is directly related to E_d as mentioned. Using different capacitor banks, the one with faster current-rise time has larger E_d at the same input energy level, and is therefore able to launch the flyer at higher velocity. The current-rise time was measured by an oscilloscope using a 50 kA: 1 V Rogowski coil encircling one terminal of

the capacitor bank. When the bank is shorted, certain amount of charge is rapidly released. The scope records the temporal evolution of the current, with the time to peak current turned as the current rise time, τ. The discharge frequency, f_c, is obtained as

$$f_c = \frac{1}{4\tau} \quad \text{Eq.4}$$

Together with the voltage trace measured using a 1000:1 probe connected across two terminals of the capacitor bank and the t_b indicated by the voltage trace or the velocity trace, the deposited energy can be obtained by Eq. 2.

2.2 VFA spot welding of Al alloy to steel

Parameters of VFAW were explored to optimize VFAW, including different energy input using different effective widths of the foil and the shape of pre-deformation. The welding couple of Aluminum 5052 with thickness of 1 mm and JSC590R steel with thickness of 1.2 mm was selected. Fig. 5 shows the implementation of VFA spot welding apparatus. The collision velocity of the flyer was measured by a PDV system.

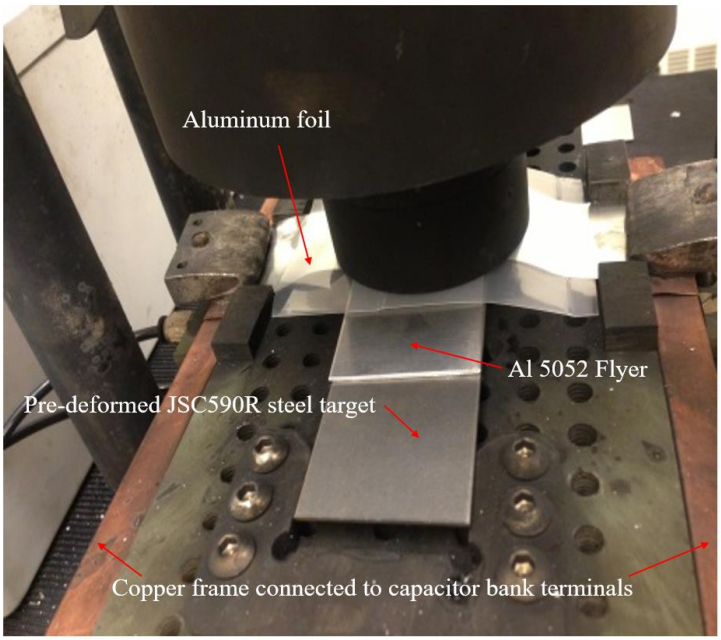

Fig. 5: The actual implementation of VFA spot welding apparatus

2.2.1 Foil geometry

The geometry of the foil to be vaporized has great effect on the process of energy deposition. Foil of bridge shape shown as Fig. 6, which can give higher energy concentration on the effective area, were used. Foils of 0.0762 mm thick with effective widths of 10.16 mm and 7.62 mm were explored.

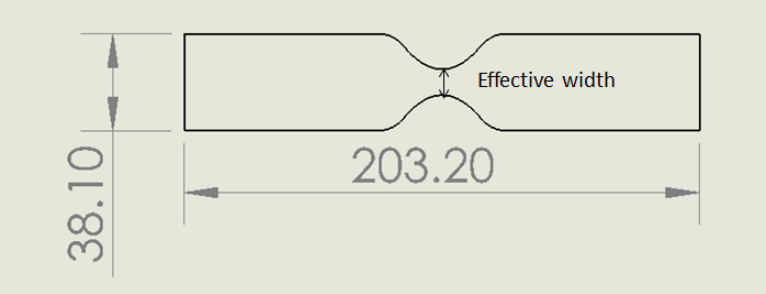

Fig. 6: Geometry of the aluminum foil (the values have the unit of millimeter)

2.2.2 Pre-deformation of the target

The target was pre-deformed before welding to give standoff for acceleration of flyer and create an impact angle. Three different shapes of pre-deformation as shown in Fig. 7.were explored.

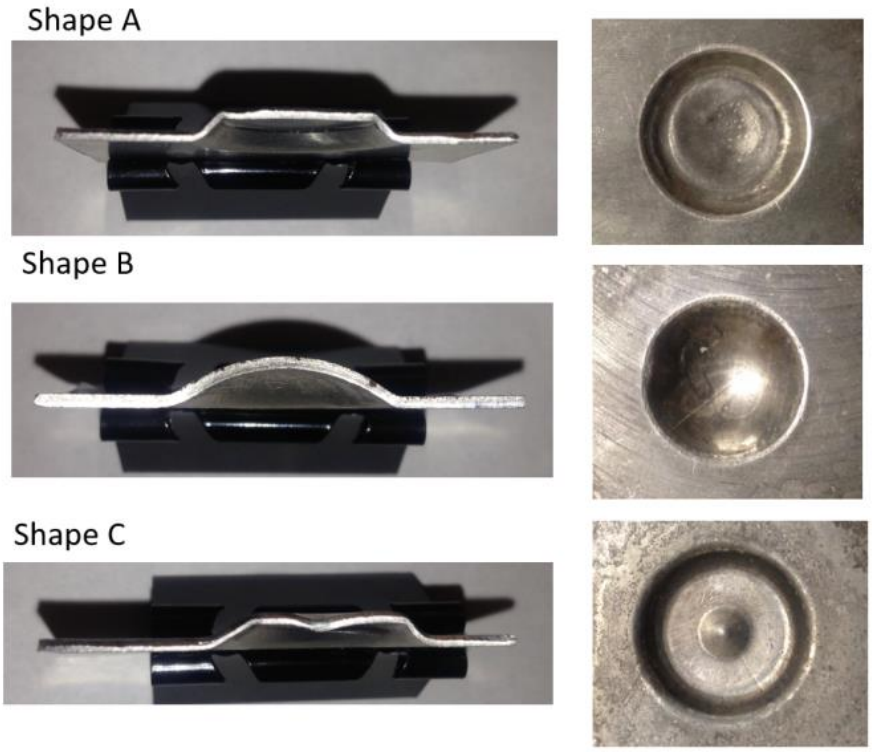

Fig. 7. Three different pre-deformation shapes A, B and C from top to bottom; section views of pre-deformed targets on the left and dies on the right

2.2.3 Measurement of the flyer velocity by a PDV system

Velocity Interferometer System for Any Reflector (VISAR), introduced by Barker and Hollenbach (1972), was a widely-used tool to measure the velocity of high speed targets. PDV is a more contemporary method utilizing readily available telecommunications devices. When the laser light is emitted towards the target by the probe, small amount of upshifted light is back-reflected as reference light and remaining light illuminates the moving target. Some of the light is reflected and Doppler-shifted and recollected by the probe. Two signals with different frequencies are mixed by a detector and interfere with each other. The difference in frequency caused by destructive interference is recorded by a high speed oscilloscope. The system in service was built in the lab and uses laser with a wavelength of 1550 nm. By analyzing the frequency shift using MATLAB software, the velocity trace of the target, v(t) can be obtained as

$$v(t) = 775 * f(t)\ \ m/s \qquad \text{Eq. 3}$$

where f(t) (GHz) is the beat frequency of the light produced by interference of original and reflected light. A schematic of a PDV system (Vivek et al. 2014b) is shown as Fig. 8.

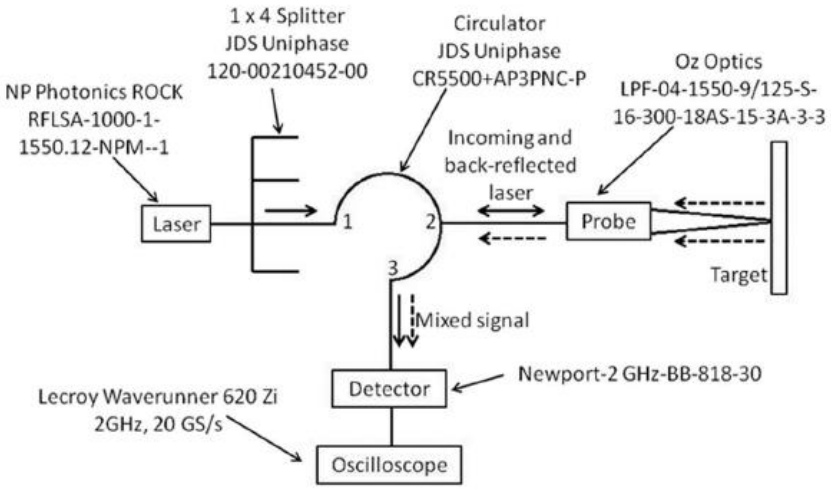

Fig. 8. A schematic of PDV system at OSU (Vivek et al., 2014b)

2.2.4 Weld quality determination: lap joint shear test and microscopic characterization

Lap joint shear tests at strain rate of 1 mm/s was used to determine the quality including strength and failure mode of the welds. In addition, the reproducibility of the weld system could be analyzed by the results of the tests for several welds created using same parameters. Fig. 9 shows the lap joint shear test of a weld.

Wavy interface morphology between two welded pieces on weld seam is generally considered to indicate optimal collision weld. As a result, morphology observation of welds under an optical microscope was performed. Micro-hardness test was performed at sample points on both base metals with different distance from weld interface. The consistency of hardness at sample points on one base metal determined if there exited heat-affected zones.

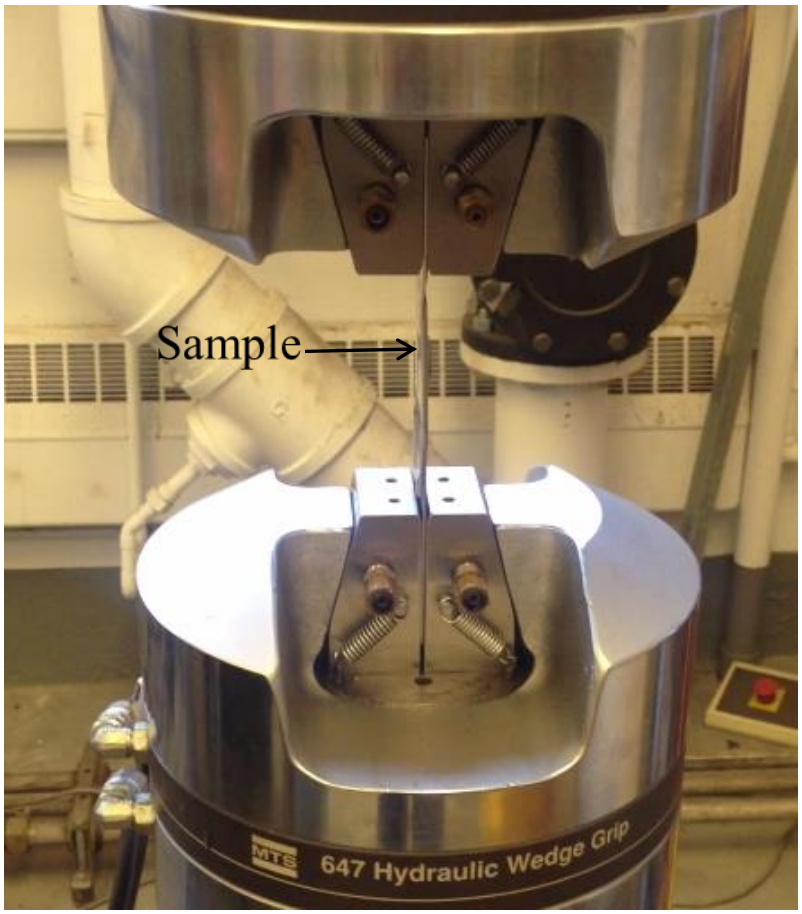

Fig. 9. A weld during lap joint shear test

Chapter 3: Results and Discussion

3.1 System characterization

A VFAW system was constructed, shown as Fig. 10. Welds of aluminum to aluminum and steel to steel at energy level below 2kJ and aluminum to steel at energy level below 3kJ were successfully created by the system. The current-rise time was measured as 7 μs and discharge frequency was calculated as 35.7 kHz. The comparison of the system and the other two capacitor banks was shown as Table 2.

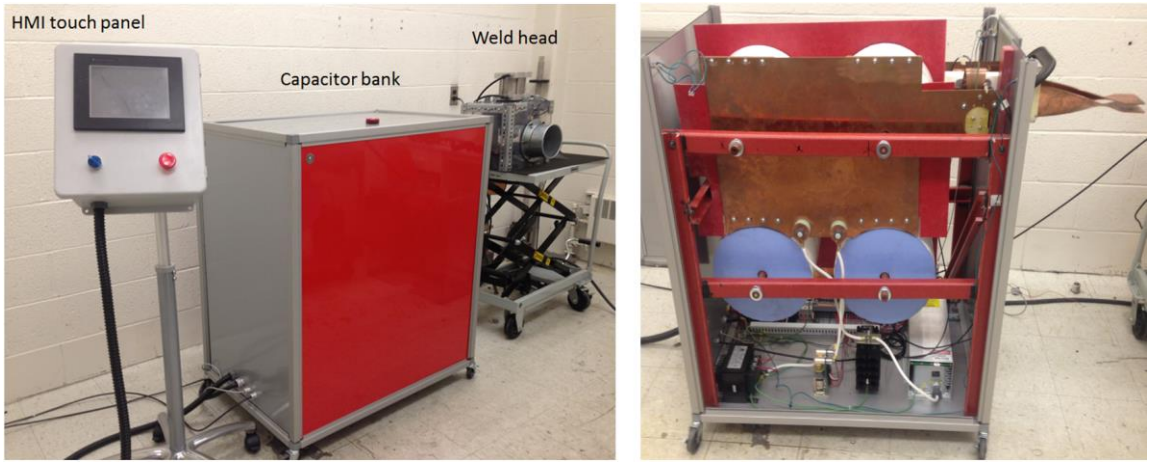

Fig. 10. The VFAW system constructed (left) and a close view of the capacitor bank (right)

Table 2. Comparison of the system and current capacitor banks

Capacitor banks	Current-rise time (μs)	Maximum input energy (kJ)	Automatic continuous shots function
System constructed	7	3.0	Yes
Current Bank 1 (CB1)	3	1.3	No
Current Bank 2 (CB2)	10	16	No

According to Table 2, the system has higher input energy than CB1 and faster current-rise than CB2. As a result, the bank has a higher maximum E_d at higher energy input than CB1, which can be proved by the fact that the system successfully welded JSC590R steel of 1.2 mm thick to the same material at energy input of 2 kJ, which CB1 was not capable of at its maximum input energy of 1.3 kJ; the weld was shown in Fig. 11. At the same input energy, the system is able to deposit more energy into the foil before it bursts than CB2 because of the shorter current-rise time, indicating higher energy efficiency. Fig. 12 shows the deposited energy of the system constructed and CB2 at same energy input of 2.6 kJ. At input energy of 2600 J, the foil vaporized by CB2 burst at 10.05 μs with E_d of 961.8 J; the foil vaporized by the system constructed burst at 6.61 μs with E_d of 2347 J, which is 2.4 times more than CB2. Furthermore, working together with a pneumatically operated welding head, the operation rate can be 1 weld/minute, which is 20 times faster than before.

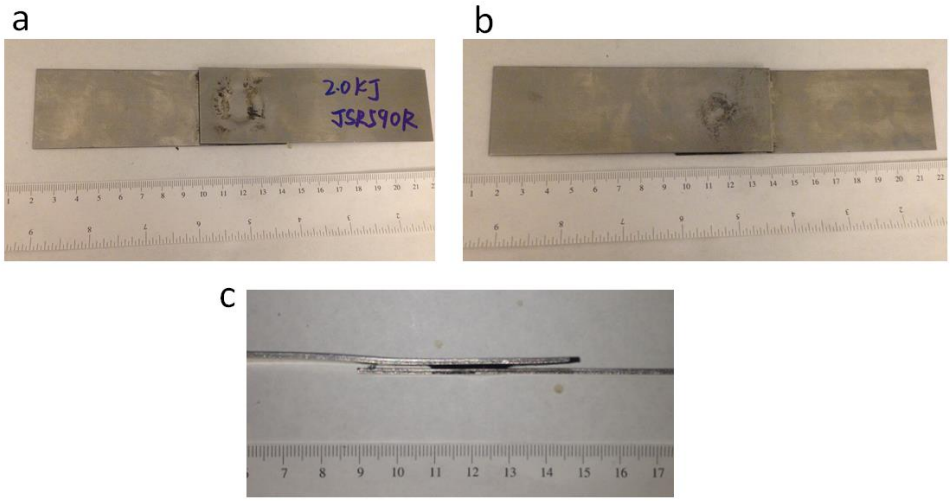

Fig. 11. A weld of steel to steel at 2kJ by the system constructed: front view (a), rear view (b), and side view (c)

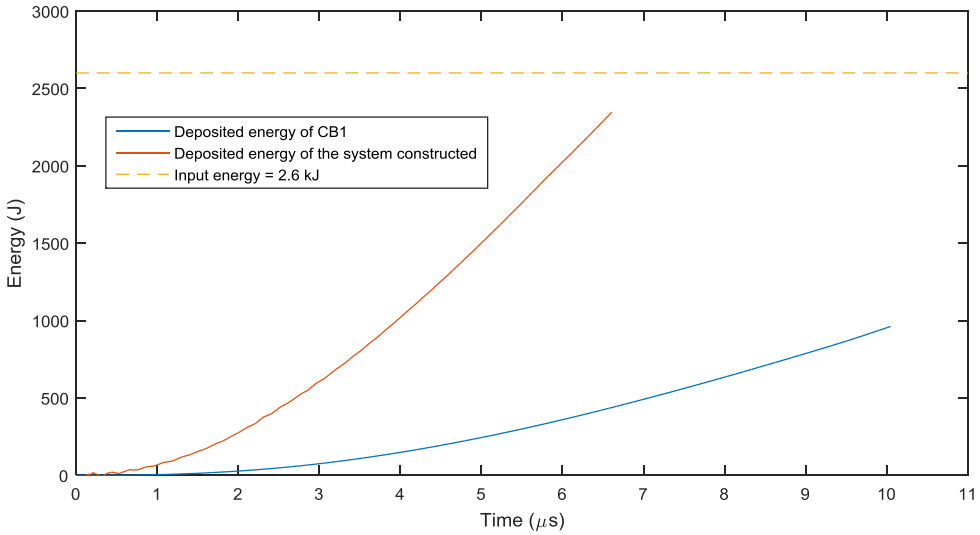

Fig. 12. Energy deposition vs. time of two capacitor banks

3.2 VFA spot welding of Al 5052 to JSC590R

Spot welds of 1 mm-thick Al 5052 to 1.2 mm-thick JSC590R were successfully created by the system constructed using VFAW parameters shown in Table 3. The welds created using parameter combinations of 4, 5 and 6 are shown in Fig. 13.

Table 3. VFAW parameters explored

Pre-deformation shape	Effective width of the foil (mm)	Input energy (kJ)	Parameter combination #
Shape A	10.16	2.8	1
		3.3	2
	7.62	2.6	3
		2.8	4
Shape B	7.62	2.6	5
Shape C	7.62	2.6	6

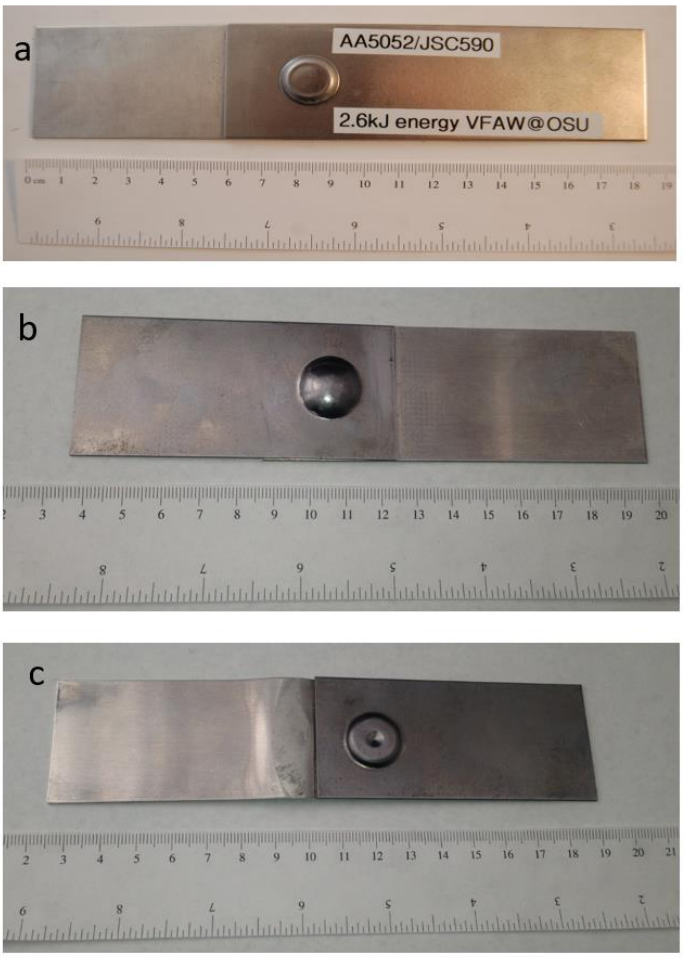

Fig. 13. VFA spot welds of aluminum to steel created using parameter combinations of (a) 1 - 4, (b) 5, and (c) 6

3.2.1 Flyer's velocity

The flyer's velocity using foils with effective width of 7.62 mm wide at input energy of 2.6 kJ is evaluated as Fig. 14. From the standoff distance of pre-deformation of shape A, the impact velocity of parameter combination 5 was estimated as 733 m/s.

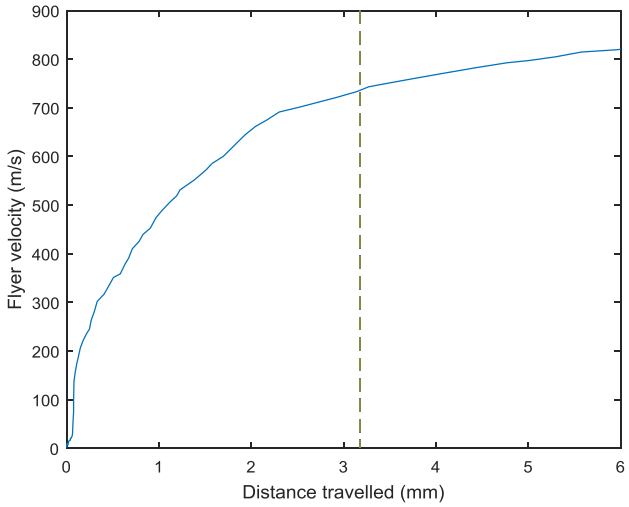

Fig. 14. Flyer's velocity evolution launched by a foil with effective width of 7.62 mm at 2.6 kJ

3.2.2 Results of lap joint shear tests

The welds of Sample 1 and Sample 4 created using parameter combination 3 after the test is shown in Fig. 15. The results of lap joint shear tests of welds created using different parameter combinations are shown in Fig. 16. The lap shear strengths of the welds created using different parameter combinations were shown in Table 4. The results in Fig. 16 indicate the reproducibility of welds in the term of lap shear strength; however, there is inconsistency in the fracture toughness of the welds, implied by narrow and wide curves in the figure.

Table 4. Lap shear strength of the welds created using different parameter combinations

Parameter combination	Lap shear strength (N)
1	5442.4 ± 208
2	5825.0 ± 117
3	5879.9 ± 364
4	5865.0 ± 84
5	6605.0 ± 479
6	6340.5 ± 775

During lap joint shear tests, a weld can yield in two different ways: one is shown in Fig. 15(a) that the nugget is pulled out by plastic deformation of weaker base metal which is aluminum, and the other one is shown in Fig. 15(b) that the interface is peeled off with little or no attached aluminum remained. Despite no huge different in the lap shear strengths of the two cases, the welds yielded in first way was able to absorb more energy during failure and therefore had a higher fracture toughness, shown as a larger area under the load-displacement diagram.

According to Table 4, using same foil geometry and pre-deformation shape, higher input energy creates stronger welds. It could result from the higher collision velocity at same impact angle. However, the input energy could also influence the impact angle because of the instantaneous plastic deformation before collision.

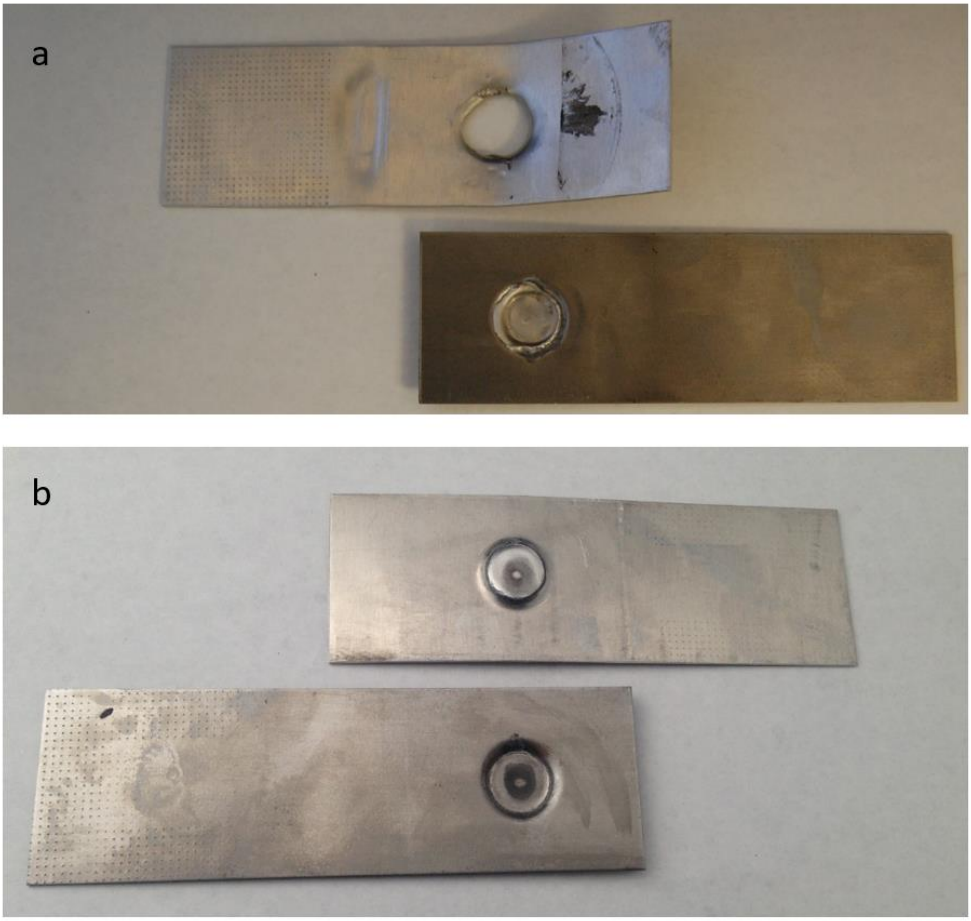

Fig. 15. Two samples created using parameter combination 3 that yielded in different ways after lap joint shear tests

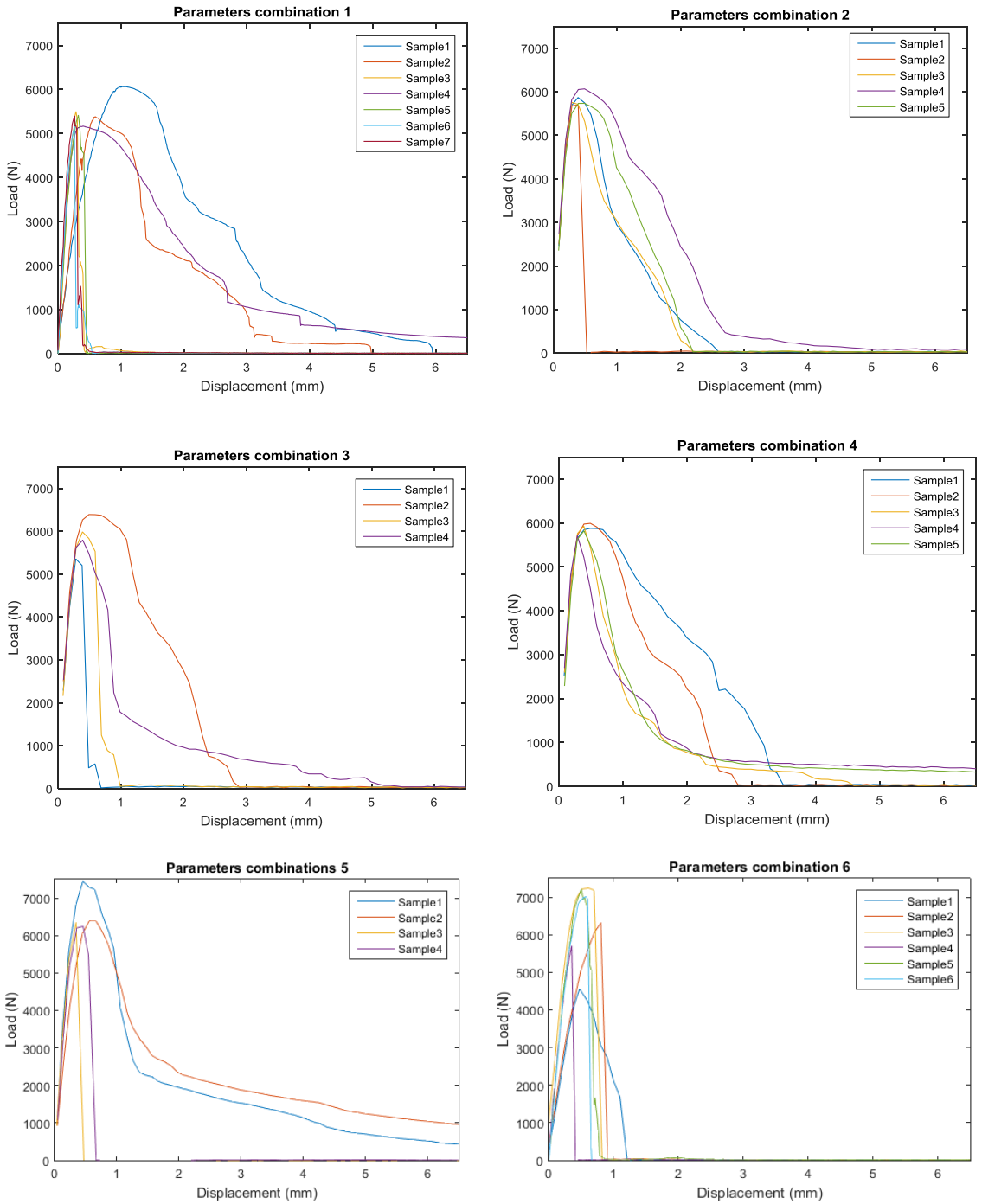

Fig. 16. Results of lap joint shear tests of welds created using parameter combinations 1-6

Welds created using pre-deformation of shape B yielded a higher lap shear strength than shape A. Fig. 17 shows two samples of the welds after the shear test, from which it can be seen that pre-deformation of shape B provided more weld area than A because of the smooth shape .The diameter of the weld spot is also slightly larger in case of shape B. In comparison, there could be even un-welded at the very center of the weld created using pre-deformation A because the flat shape in the middle is not able to provide sufficient impact angles.

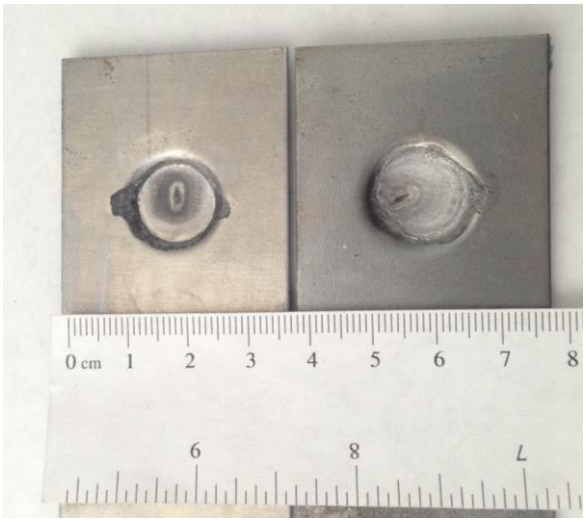

Fig. 17. Comparison of the welds after lap joint shear test created using parameter combinations 3 (left) and 5 (right)

The foil with effective width 7.62 mm worked better than 10.16 mm. Fig. 18 shows a possible mechanism of the effect of effective widths of the foils on collision welding. With a smaller effective width, the plasma generated with high pressure impulse forces on smaller area of the flyer, causing a sharper shape of the flyer on collision. As a consequence, the collision angle is higher, which creates a weld with less IMC.

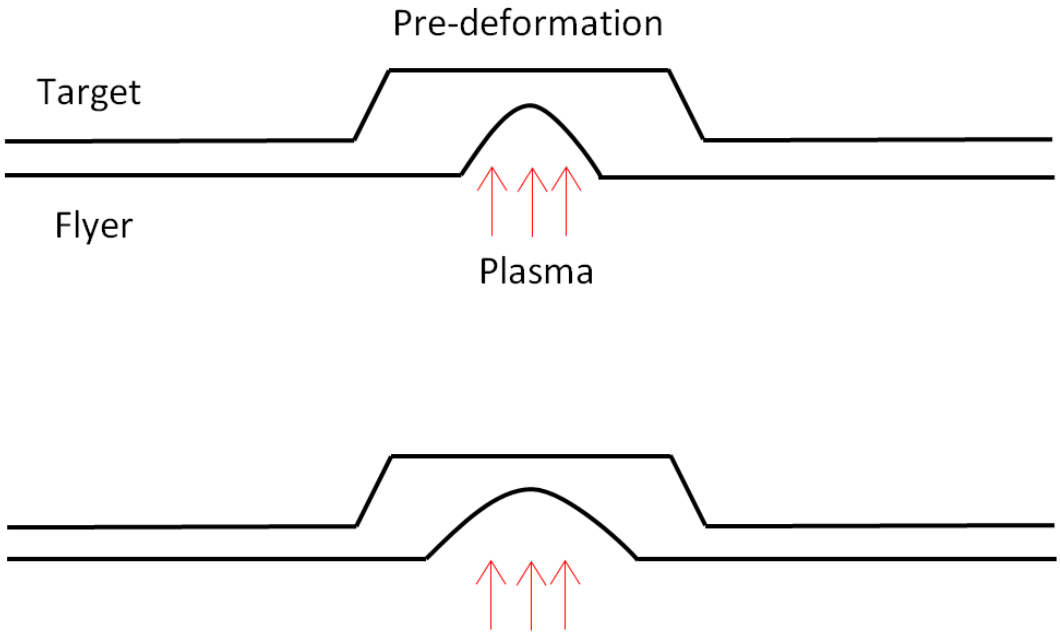

Fig. 18. Schematic of possible mechanism of the effect of effective width of foils

3.2.2 Microscopic characterization

Sectional micrographs of different position of a weld created using parameter combinations 3 and 5 are shown in Fig. 19, and Fig. 20. Wavy pattern on the seam and continuous layers of IMC between aluminum and steel were observed. For deformation of shape A, more IMC was created in the center area (region a) because of the very low collision angle while area around slope on the edge (region c) is IMC free. For deformation of shape B, although it was designed to reduce the flat shape, there was still IMC dominating the weld. Moreover, as there was no deep slope in shape B to provide a high impact angle for strong welds, given the weld area of the weld created using pre-deformation shape B was twice more than shape A according to Fig. 16, the increase of

lap shear strength could be due to the result of the increase of weld area over the decrease of strength per unit area.

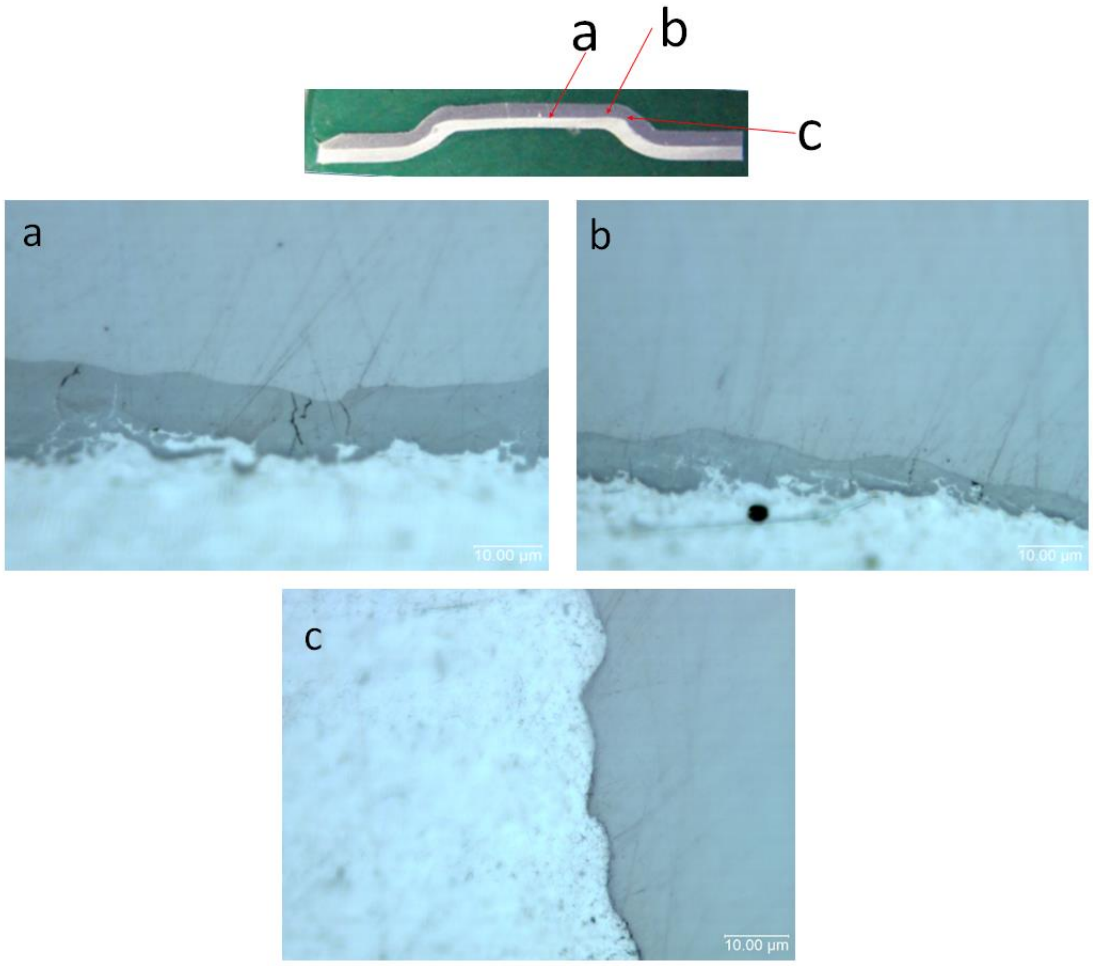

Fig. 19. Sectional micrographs of different positions (region a, b, and c) of a weld created using parameters combination 3

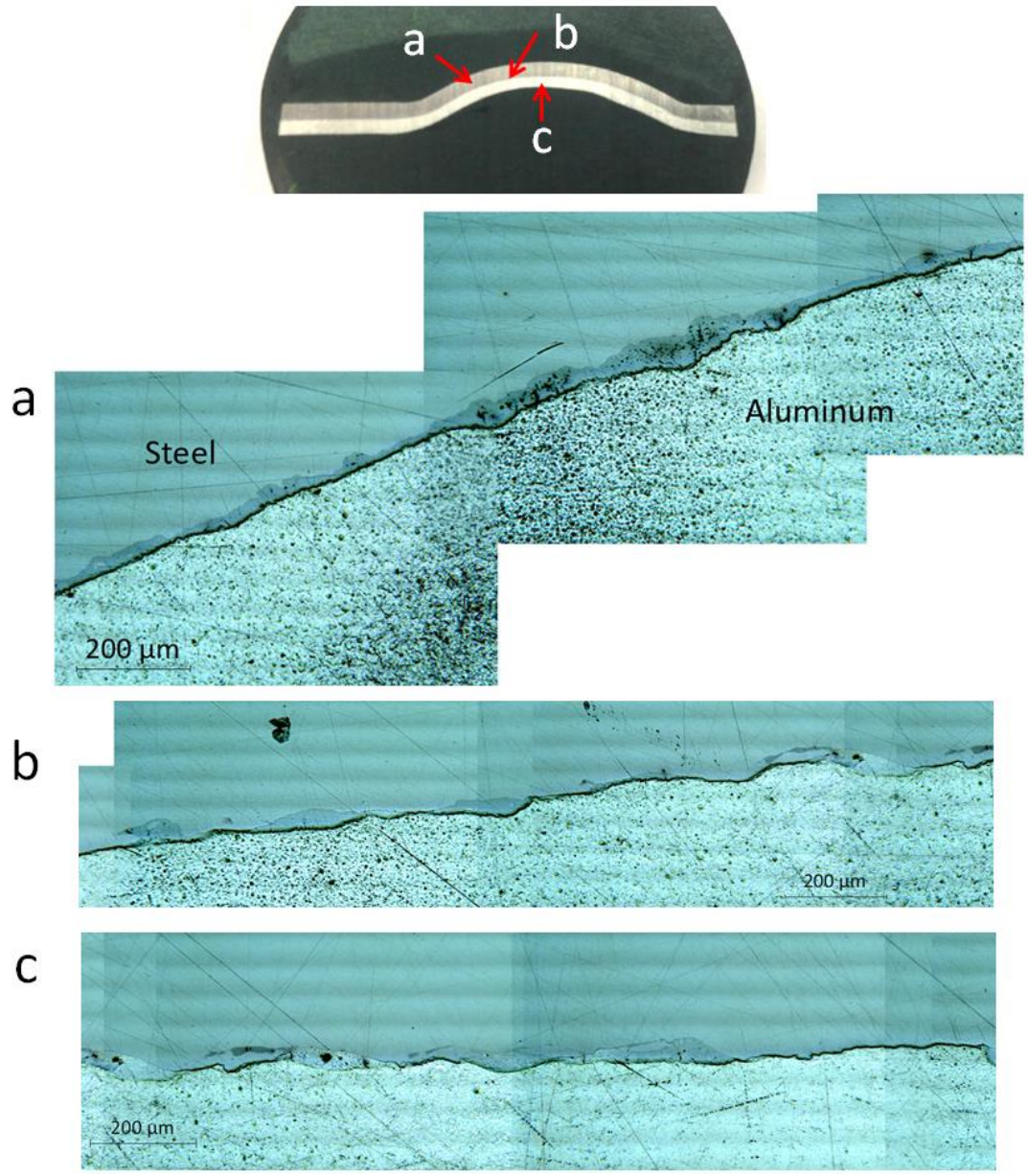

Fig. 20. Sectional micrographs of different positions of a weld created using parameter combination 5

3.2.3 Micro-hardness test

The result of hardness test of a weld using parameter combination 5 was shown in Table 5. The indentations after the test are shown in Fig. 21. According to the values of Vickers hardness at sample points with different distance from the weld interface, both the hardness of JSC590R steel and Al 5052 has a good consistency and is independent on the distance between the sample points and the weld interface. It indicates that there was no heat-affected zone caused by heat-induced recrystallization on base metals, which achieved one of goals of VFAW as mentioned.

Table 5. Results of micro-hardness tests

Base metal	Sample point	Vickers hardness (HV)	
JSC590R steel	a	203	Average = 209.8±2.9
	b	210	
	c	215	
	d	209	
	e	212	
	f	210	
Al 5052	g	73	Average = 70.0±2.7
	h	69	
	i	72	
	j	66	

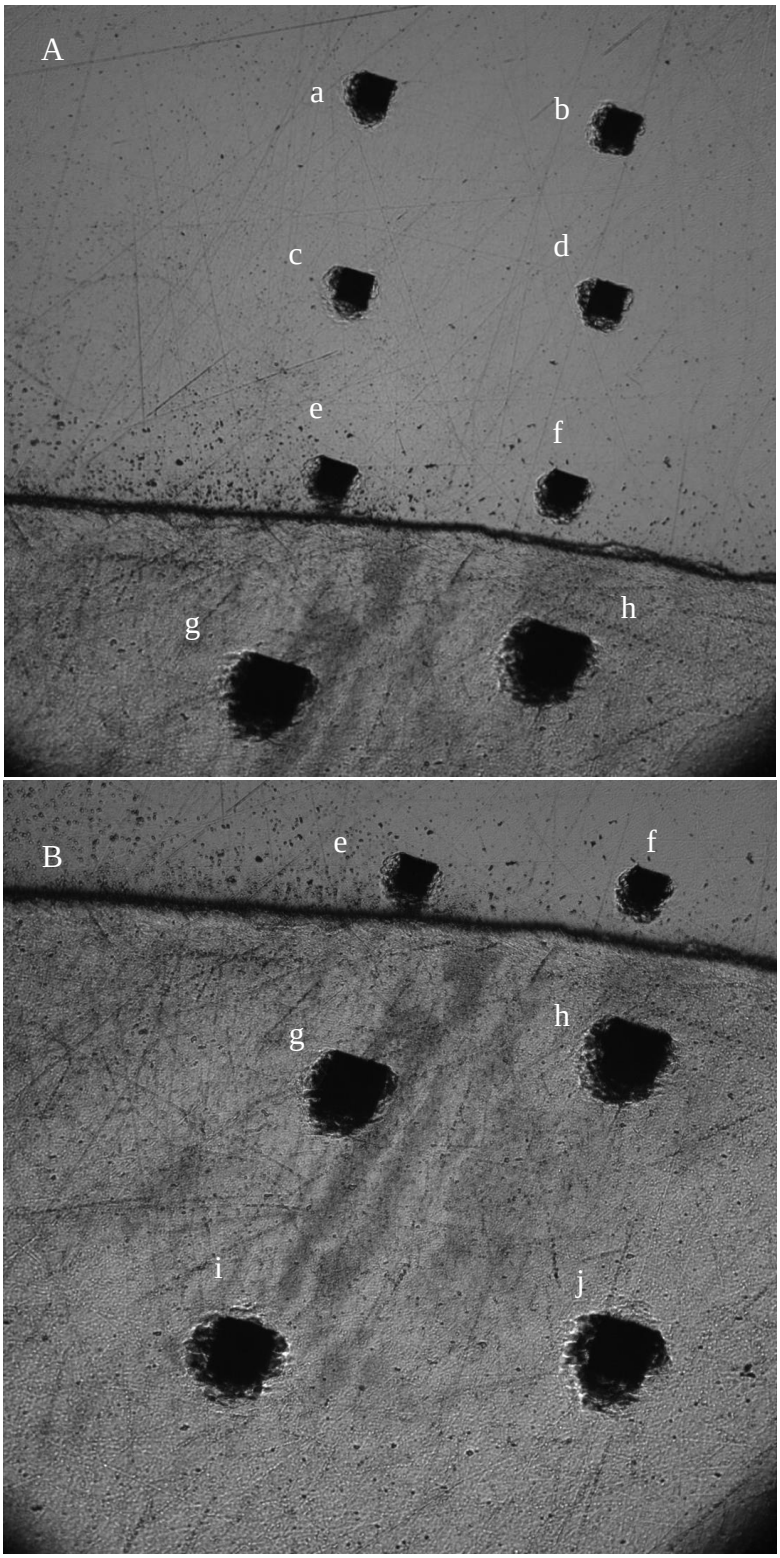

Fig. 21. (A) Micro-hardness test of a weld created using parameters combination 5 and (B) continued.

Chapter 4: Conclusion

A VFAW system with high operational efficiency and the function of automatic continuous shots as well as capability of higher energy deposition than previously available systems was constructed.

VFAW is proved be a viable and energy-efficient method for spot welding of aluminum 5052 to JSC590R steel without producing heat-affected zone. Welding processing parameters such as input energy, foil geometry, and pre-deformation geometry greatly affect the microstructure and quality of the weld. The welds which yielded by pulling out the nugget has higher fracture toughness than the welds yielded by peeling off the interface. Continuous IMC layer was created on collision due to too high collision velocity and insufficient impact angle. Welds created at higher input energy shows higher lap shear strength and higher fracture toughness caused by the higher flyer impact velocity Aluminum foils with smaller effective width of 7.62mm created stronger welds as a result of sharper flyer shape on collision, which can provide more collision angle and therefore reduce the creation of IMC. Pre-deformation shape B, which is more curved, created welds with higher lap shear strength due to its more weld area; however, the curved shape decreases the strength per weld area by decreasing the collision angle.

No matter which shape of pre-deformation is used, the brittle IMC dominated over good welding area in a weld mostly because of the insufficient impact angle. There is much scope for further optimization of the geometry of pre-deformation shape and of the aluminum foil during the VFAW process.

Chapter 5: Future Work

The future work will be focusing on the geometry of the foil and the geometry of the pre-deformation. The pre-deformation shape controlling the impact angle still needs to be further optimized as IMC was dominating the weld. Shape evolution of the flyer as it accelerates by vaporizing foil needs to be researched by simulation and PDV experiments, which can greatly help to optimize the foil geometry and pre-deformation shape. Also, weld window of aluminum to steel can guide the optimization of the pre-deformation shape. In addition, the identification of Fe-Al IMC can be done to help to explore the process of the IMC creation.

References

Barker, L. M., & Hollenbach, R. E. (1972). Laser interferometer for measuring high velocities of any reflecting surface. *Journal of Applied Physics*, *43*(11), 4669-4675.

Ben-Artzy, A., Stern, A., Frage, N., Shribman, V., Sadot, O., 2010. Wave formationmechanism in magnetic pulse welding. Int. J. Impact Eng. 37 (4), 397–404,http://dx.doi.org/10.1016/j.ijimpeng.2009.07.008.

Briskham, P., Blundell, N., Han, L., Hewitt, R., Young, K., & Boomer, D. (2006). Comparison of self-pierce riveting, resistance spot welding and spot friction joining for aluminium automotive sheet. SAE SP, 2034, 105.

Chau, H.H., Dittbenner, G., Hofer, W.W., Honodel, C.A., Steinberg, D.J., Stroud, J.R.,Weingart, R.C., Lee, R.S., 1980. Electric gun: a versatile tool for high-pressureshock-wave research. Rev. Sci. Instrum. 51 (12), 1676–1681, http://dx.doi.org/10.1063/1.1136155.

Cho, C., Murai, K., Suzuki, T., Suematsu, H., Jiang, W., & Yatsui, K. (2004). Enhancement of energy deposition in pulsed wire discharge for synthesis of nanosized powders. *Plasma Science, IEEE Transactions on*, *32*(5), 2062-2067.

Grigoriev, A. N., & Pavlenko, A. V. (2009). Pressure generated by the electric explosion of metal foils. *Technical Physics Letters*, *35*(9), 865-868.

Golovashchenko, S. F. (2007). Material formability and coil design in electromagnetic forming. Journal of Materials Engineering and Performance, 16(3), 314-320.

Guenther, A. H., Wunsch, D. C., & Soapes, T. D. (1962). Acceleration of thin plates by exploding foil techniques. In *Exploding Wires* (pp. 279-298). Springer US.

Hahn, M., Weddeling, C., Taber, G., Vivek, A., Daehn, G. S., & Tekkaya, A. E. (2016). Vaporizing foil actuator welding as a competing technology to magnetic pulse welding. *Journal of Materials Processing Technology*, *230*, 8-20.

Keller, D. V., & Penning Jr, J. R. (1962). Exploding foils—the production of plane shock waves and the acceleration of thin plates. In *Exploding wires* (pp. 263-277). Springer US.

Kore, S.D., Imbert, J., Worswick, M.J., Zhou, Y., 2009. Electromagnetic impactwelding of Mg to Al sheets. Sci. Technol. Weld. Join. 14 (6), 549–553, http://dx.doi.org/10.1179/136217109X449201.

Kotov, Y. A., & Samatov, O. M. (1999). Production of nanometer-sized ain powders by the exploding wire method. *Nanostructured materials*, *12*(1), 119-122.

Mori, K., Bay, N., Fratini, L., Micari, F., Tekkaya, A.E., 2013. Joining by plasticdeformation. CIRP Ann.—Manuf. Technol. 62 (2), 673–694, http://dx.doi.org/10.1016/j.cirp.2013.05.004.

Okagawa, K., Aizawa, T., 2004. Impact Seam Welding with Magnetic Pressurefor Aluminum Sheets, Explosion, Shock Wave and Hypervelocity Phenomenain Materials, Vol. 465–466. Zurich-Uetikon: Trans Tech Publications Ltd., pp.231–236.

Ozaki, H., & Kutsuna, M. (2012). *Dissimilar Metal Joining of Zinc Coated Steel and Aluminum Alloy by Laser Roll Welding*. INTECH Open Access Publisher.

Suzuki T, Keawchai K, Jiang W H. Nanosize Al2O3 powder production by pulsed wire discharge[J]. Jpn, J. Appl. Phys., Vol.40, 2001: 1073

Tucker, T. J., & Stanton, P. L. (1975). Electrical Gurney energy: A new concept in modeling of energy transfer from electrically exploded conductors.*Sandia National Laboratories Report SAND*, 75-0244. Vivek, A., Hansen, S. R., & Daehn, G. S. (2014b).

Vivek, A., Liu, B. C., Hansen, S. R., & Daehn, G. S. (2014a). Accessing collision welding process window for titanium/copper welds with vaporizing foil actuators and grooved targets. *Journal of Materials Processing Technology*, *214*(8), 1583-1589.

Vivek, A., Hansen, S. R., & Daehn, G. S. (2014b). High strain rate metalworking with vaporizing foil actuator: Control of flyer velocity by varying input energy and foil thickness. *Review of Scientific Instruments*, *85*(7), 075101.

Vivek, A., Hansen, S.R., Liu, B.C., Daehn, G.S., 2013. Vaporizing foil actuator: a toolfor collision welding. J. Mater. Process. Technol. 213 (12), 2304–2311, http://dx.doi.org/10.1016/j.jmatprotec.2013.07.006.

Wang, G., Zhao, J., Luo, B., Jiang, J., 2011. Magnetohydrodynamics of metallic foilelectrical explosion and magnetically driven quasi-isentropic compression. In:Schulz, H. (Ed.), Hydrodynamics—Advanced Topics. InTech, 347-378, ISBN978-953-307-596-9.

Weingart, R. C. (1980). Electric gun: applications and potential. *Energy and Technology Review, LLNL, UCRL-52000-90-2*, *28*.

Watanabe, M., Kumai, S., Aizawa, T., 2006. Interfacial Microstructure of MagneticPressure Seam Welded Al–Fe, Al–Ni and Al–Cu Lap Joints, Aluminium Alloys, Pts1 and 2: Research Through Innovation and Technology, Vol. 519–521. Zurich-Uetikon: Trans Tech Publications Ltd., pp. 1145–1150.

Yasuyama, M., Ogawa, K., & Taka, T. (1996). Spot welding of aluminium and steel sheet with an insert of aluminium clad steel sheet: dissimilar metal joining of aluminium and steel sheet (1st report).

Appendix A: Spot welds of Al 5052 to JSC590R steel (other views)

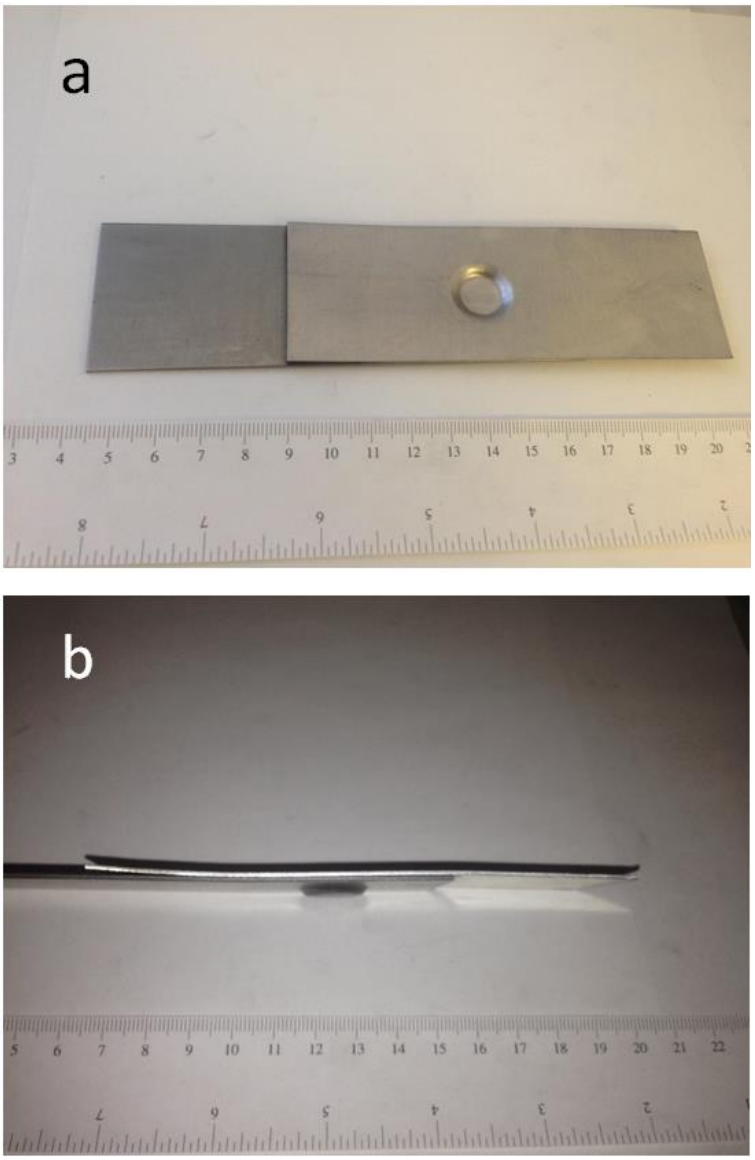

Fig. 22. Rear view (a) and side view (b) of a weld created using parameters combination 4

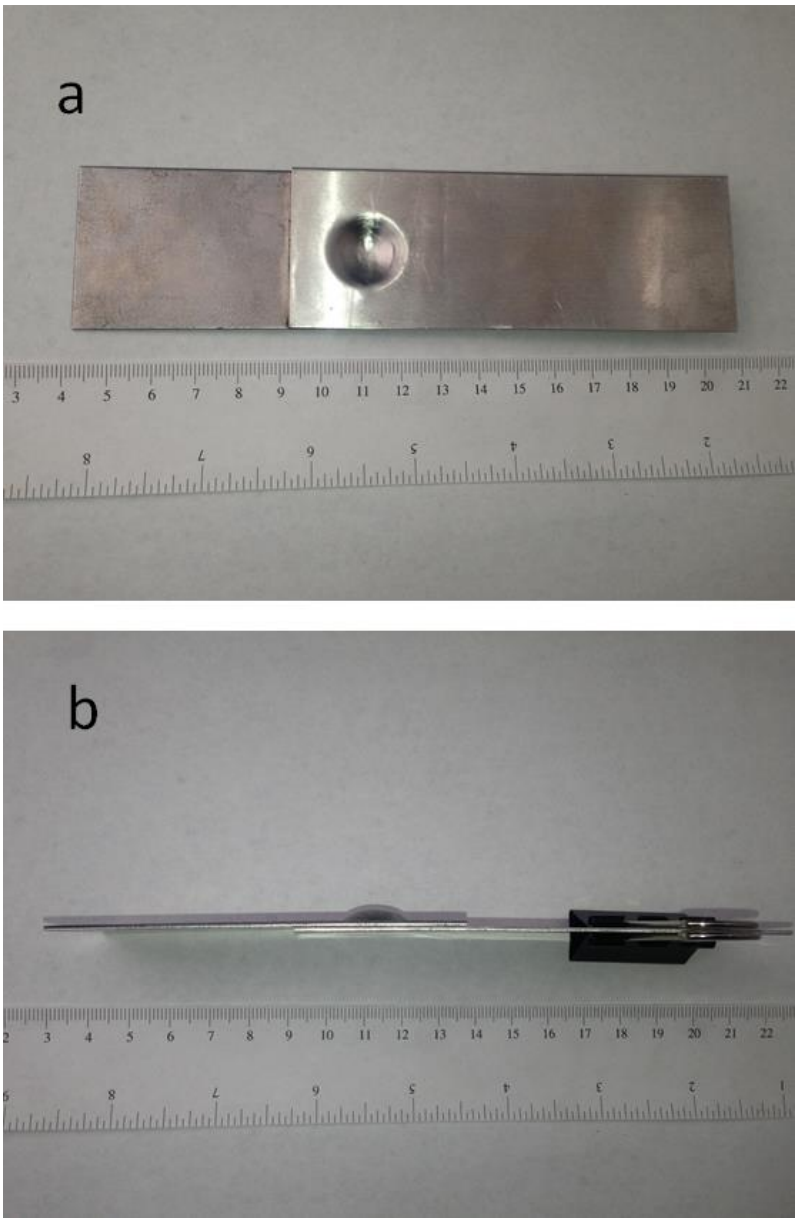

Fig. 23. Rear view (a) and side view (b) of a weld created using parameters combination 5

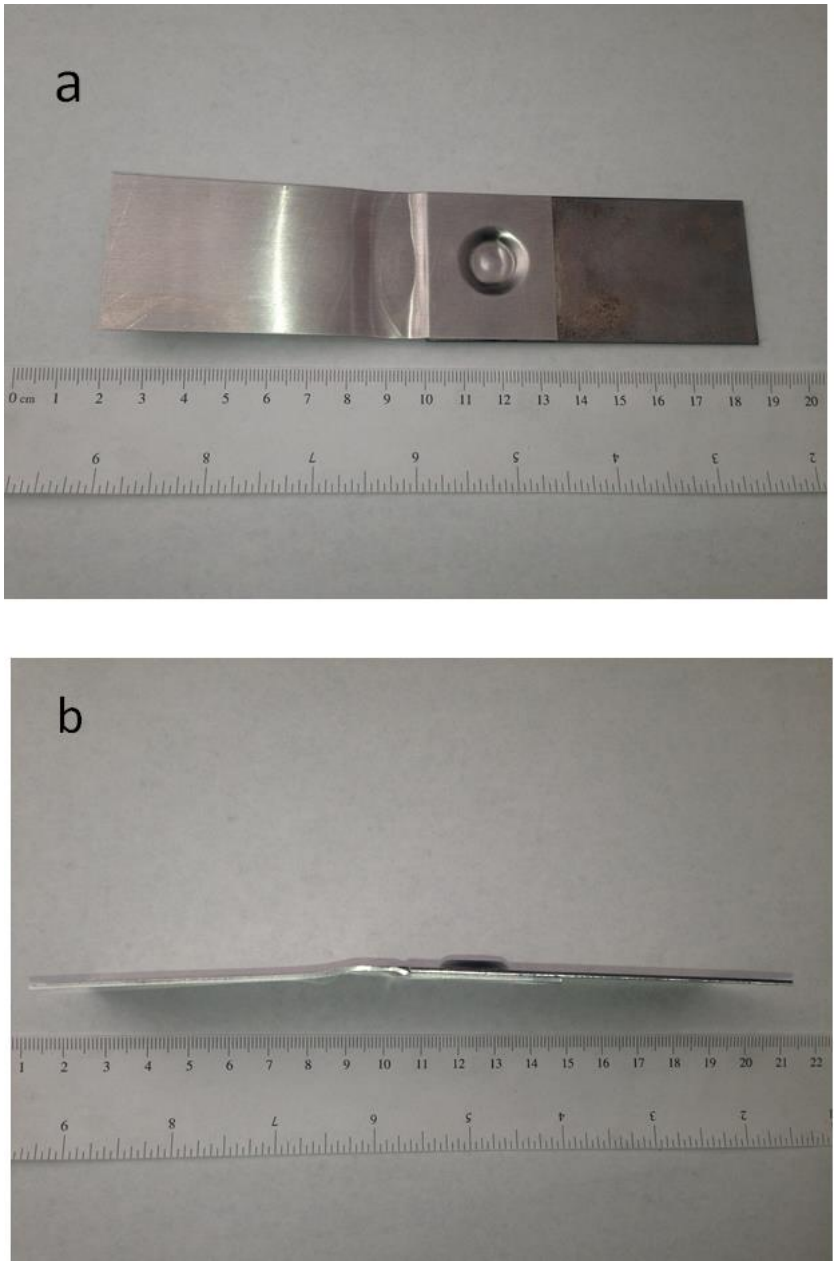

Fig. 24. Rear view (a) and side view (b) of a weld created using parameter combination 6

Appendix B: Sectional micrographs of some welds

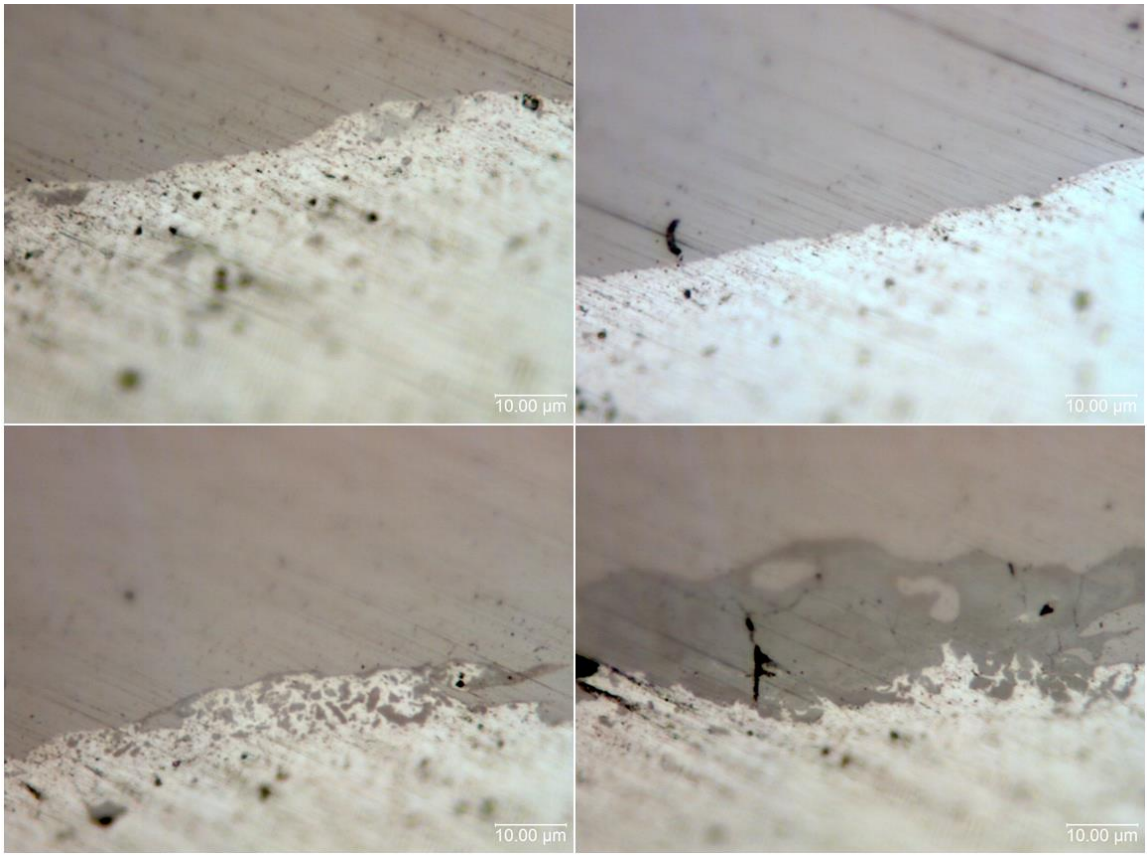

Fig. 25. Sectional micrographs of different positions of a weld created using parameter combination 2

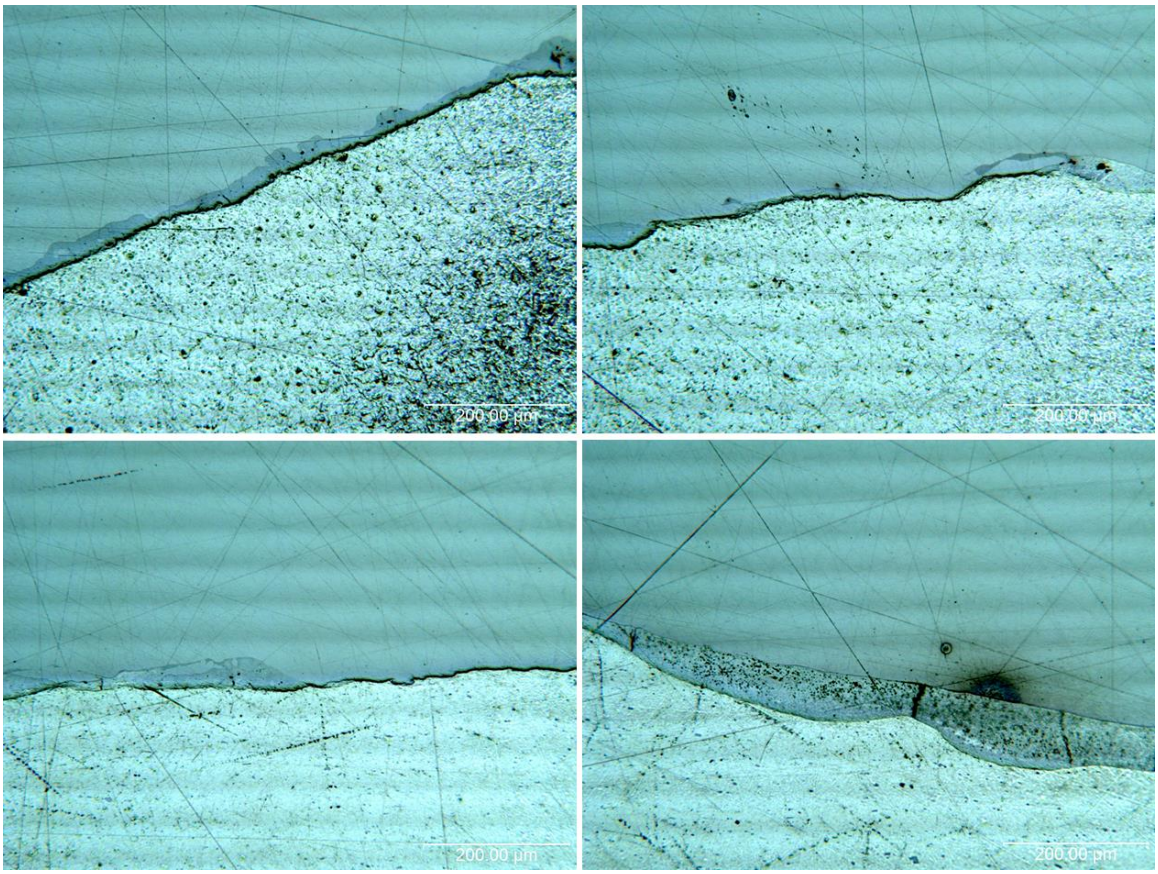

Fig. 26. Sectional micrographs of different positions of a weld created using parameter combination 5

Appendix C: More about the VFAW system constructed

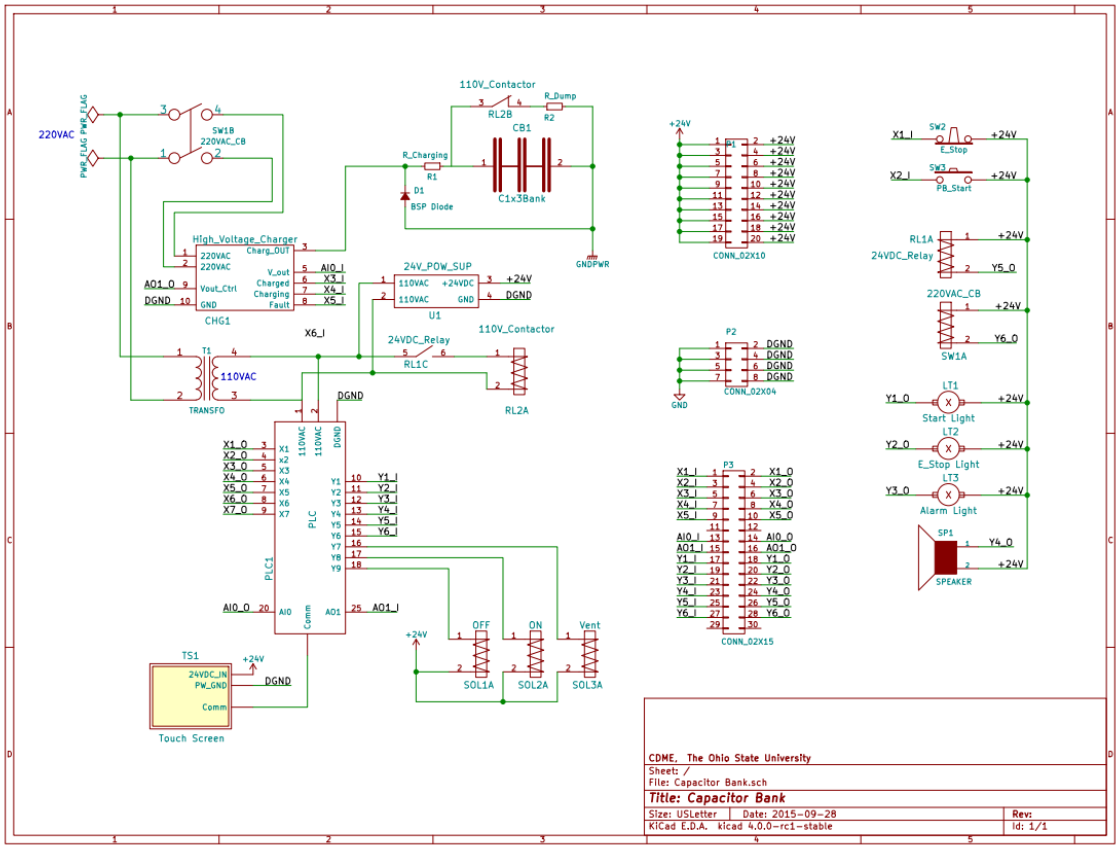

Fig. 27. Circuit diagram of the VFAW system constructed

Fig. 28. PLC program of the VFAW system (Page 47–Page 52)

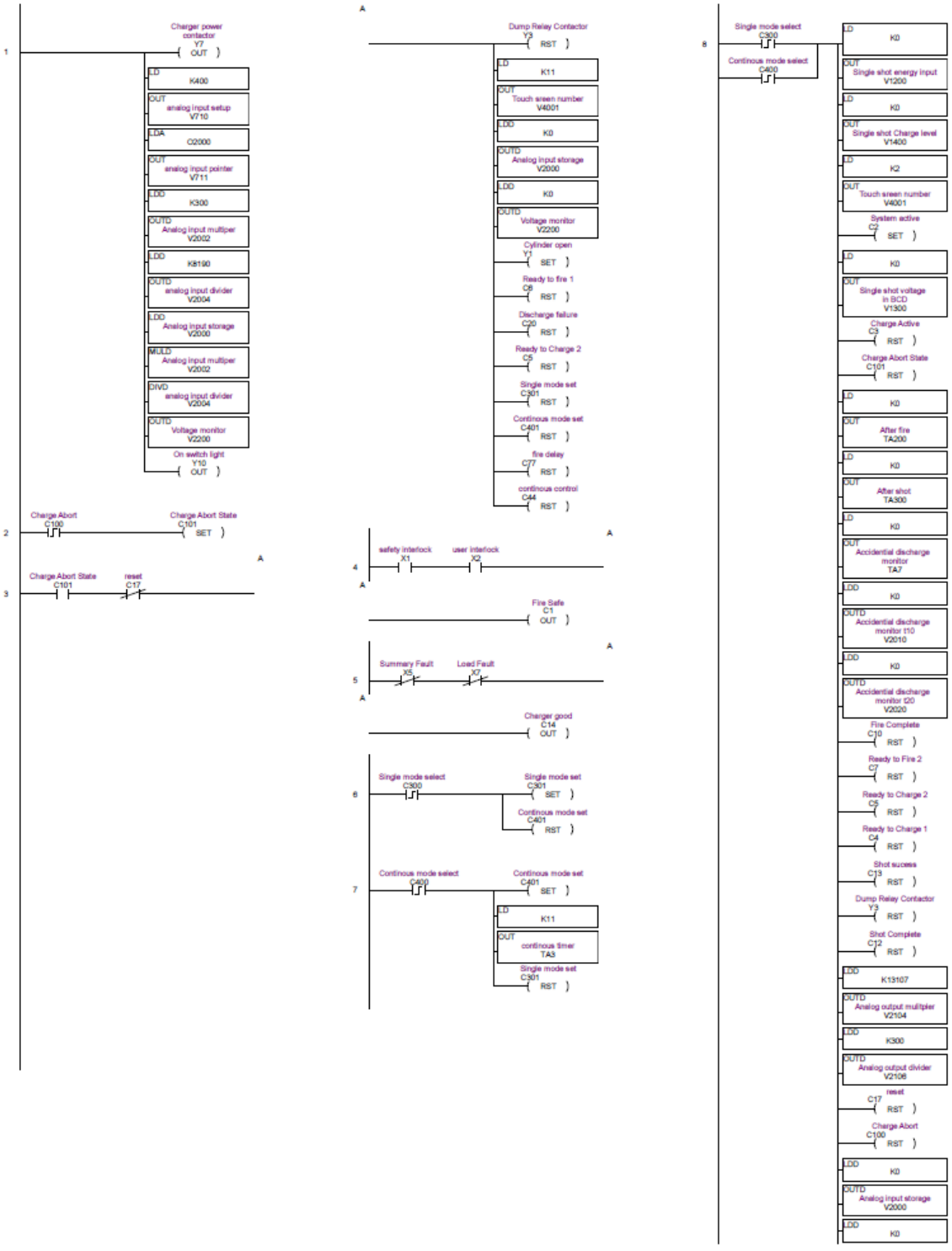

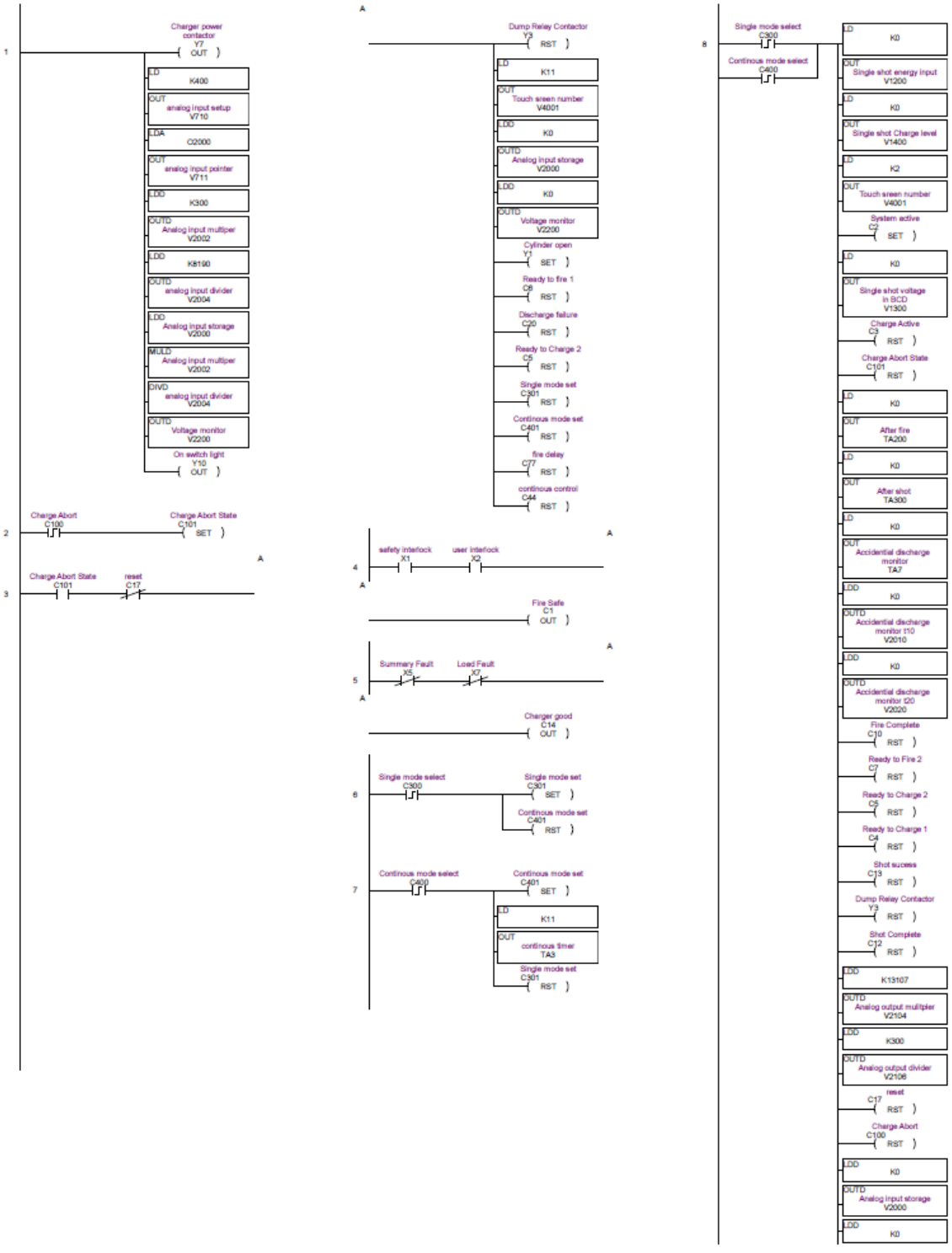
1
Charger power contactor Y7 OUT
LD K400
OUT analog input setup V710
LDA C2000
OUT analog input pointer V711
LDD K300
OUTD Analog input multiper V2002
LDD K8190
OUTD analog input divider V2004
LDD Analog input storage V2000
MULD Analog input multiper V2002
DIVD analog input divider V2004
OUTD Voltage monitor V2200
On switch light Y10 OUT
2
Charge Abort C100
Charge Abort State C101 SET
A
3
Charge Abort State C101
reset C17
A
Dump Relay Contactor Y3 RST
LD K11
OUT Touch sreen number V4001
LDD K0
OUTD Analog input storage V2000
LDD K0
OUTD Voltage monitor V2200
Cylinder open Y1 SET
Ready to fire 1 C8 RST
Discherge failure C20 RST
Ready to Charge 2 C5 RST
Single mode set C301 RST
Continous mode set C401 RST
fire delay C77 RST
continous control C44 RST
A
4
safety interlock X1
user interlock X2
A
Fire Safe C1 OUT
A
5
Summery Fault X5
Load Fault X7
A
Charger good C14 OUT
6
Single mode select C300
Single mode set C301 SET
Continous mode set C401 RST
7
Continous mode select C400
Continous mode set C401 SET
LD K11
OUT continous timer TA3
Single mode set C301 RST
8
Single mode select C300
Continous mode select C400
LD K0
OUT Single shot energy input V1200
LD K0
OUT Single shot Charge level V1400
LD K2
OUT Touch sreen number V4001
System active C2 SET
LD K0
OUT Single shot voltage in BCD V1300
Charge Active C3 RST
Charge Abort State C101 RST
LD K0
OUT After fire TA200
LD K0
OUT After shot TA300
LD K0
OUT Accidential discherge monitor TA7
LDD K0
OUTD Accidential discherge monitor t10 V2010
LDD K0
OUTD Accidential discherge monitor t20 V2020
Fire Complete C10 RST
Ready to Fire 2 C7 RST
Ready to Charge 2 C5 RST
Ready to Charge 1 C4 RST
Shot success C13 RST
Dump Relay Contactor Y3 RST
Shot Complete C12 RST
LDD K13107
OUTD Analog output mulitpler V2104
LDD K300
OUTD Analog output divider V2106
reset C17 RST
Charge Abort C100 RST
LDD K0
OUTD Analog input storage V2000
LDD K0

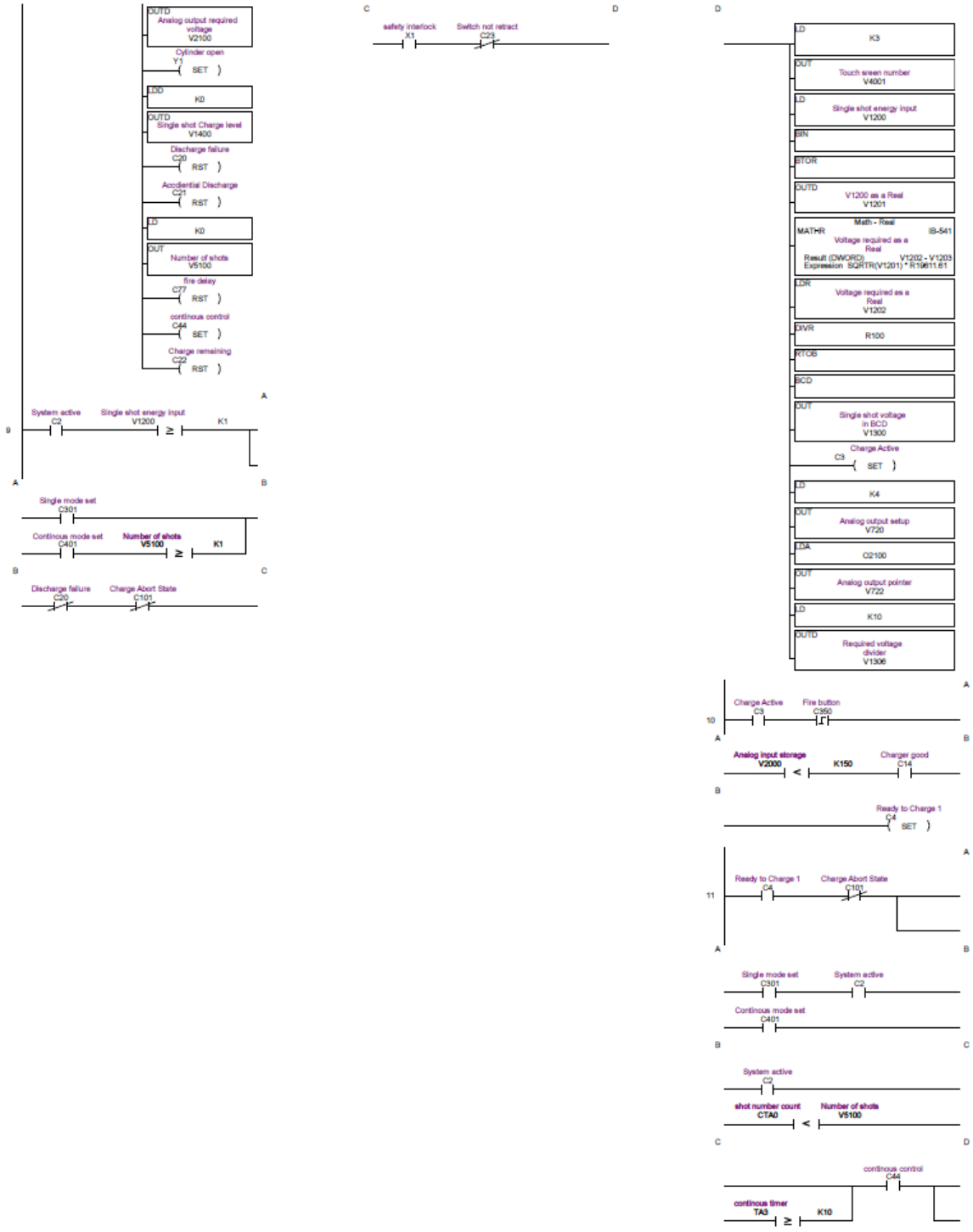
OUTD
Analog output required voltage
V2100
Cylinder open
Y1
SET
LDD
K0
OUTD
Single shot Charge level
V1400
Discharge failure
C20
RST
Accidential Discharge
C21
RST
LD
K0
OUT
Number of shots
V5100
fire delay
C77
RST
continous control
C44
SET
Charge remaining
C22
RST
A
9
System active
C2
Single shot energy input
V1200
≥
K1
A
B
Single mode set
C301
Continous mode set
C401
Number of shots
V5100
≥
K1
B
C
Discharge failure
C20
Charge Abort State
C101
C
D
safety interlock
X1
Switch not retract
C23
D
LD
K3
OUT
Touch sreen number
V4001
LD
Single shot energy input
V1200
BIN
BTOR
OUTD
V1200 as a Real
V1201
Math - Real
MATHR
IB-541
Voltage required as a Real
Result (DWORD)
V1202 - V1203
Expression
SQRTR(V1201) * R10611.61
LDR
Voltage required as a Real
V1202
DIVR
R100
RTOB
BCD
OUT
Single shot voltage in BCD
V1300
Charge Active
C3
SET
LD
K4
OUT
Analog output setup
V720
LDA
O2100
OUT
Analog output pointer
V722
LD
K10
OUTD
Required voltage divider
V1306
A
10
Charge Active
C3
Fire button
C350
A
B
Analog input storage
V2000
<
K150
Charger good
C14
B
Ready to Charge 1
C4
SET
A
11
Ready to Charge 1
C4
Charge Abort State
C101
A
B
Single mode set
C301
System active
C2
Continous mode set
C401
B
C
System active
C2
shot number count
CTA0
<
Number of shots
V5100
C
D
continous control
C44
continous timer
TA3
≥
K10

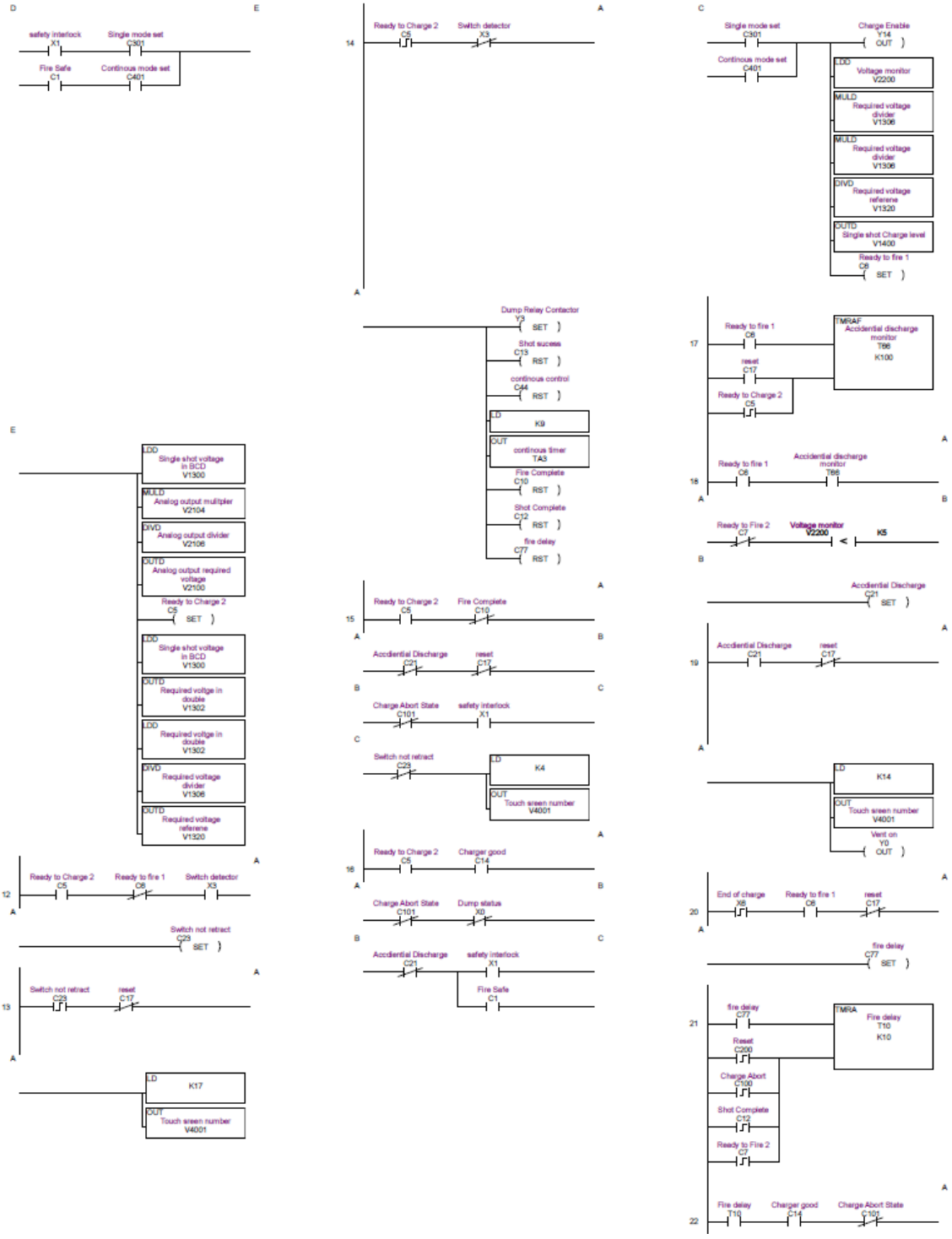
safety interlock
X1
Single mode set
C301
Fire Safe
C1
Continous mode set
C401
Ready to Charge 2
C5
Switch detector
X3
Dump Relay Contactor
Y3
SET
Shot sucess
C13
RST
continous control
C44
LD
K9
OUT
continous $mer
TA3
Fire Complete
C10
Shot Complete
C12
fire delay
C77
LDD
Single shot voltage in BCD
V1300
MULD
Analog output multiplier
V2104
DIVD
Analog output divider
V2106
OUTD
Analog output required voltage
V2100
Ready to Charge 2
C5
SET
LDD
Single shot voltage in BCD
V1300
OUTD
Required voltge in double
V1302
LDD
Required voltge in double
V1302
DIVD
Required voltage divider
V1306
OUTD
Required voltage referene
V1320
Ready to Charge 2
C5
Ready to fire 1
C6
Switch detector
X3
Switch not retract
C29
SET
reset
C17
LD
K17
OUT
Touch sreen number
V4001
Charge Abort State
C101
safety interlock
X1
LD
K4
OUT
Touch sreen number
V4001
Charger good
C14
Dump status
X0
Accidential Discharge
C21
Fire Safe
C1
Single mode set
C301
Charge Enable
Y14
OUT
Continous mode set
C401
LDD
Voltage monitor
V2200
MULD
Required voltage divider
V1306
MULD
Required voltage divider
V1306
DIVD
Required voltage referene
V1320
OUTD
Single shot Charge level
V1400
Ready to fire 1
C6
SET
TMRAF
Accidential discharge monitor
T66
K100
reset
C17
Ready to Charge 2
C5
Ready to Fire 2
C7
Voltage monitor
V2200
K5
Accidential Discharge
C21
SET
LD
K14
OUT
Touch sreen number
V4001
Vent on
Y0
OUT
End of charge
X6
fire delay
C77
TMRA
Fire delay
T10
K10
Reset
C200
Charge Abort
C100
Shot Complete
C12
Ready to Fire 2
C7
Fire delay
T10
Charger good
C14
Charge Abort State
C101

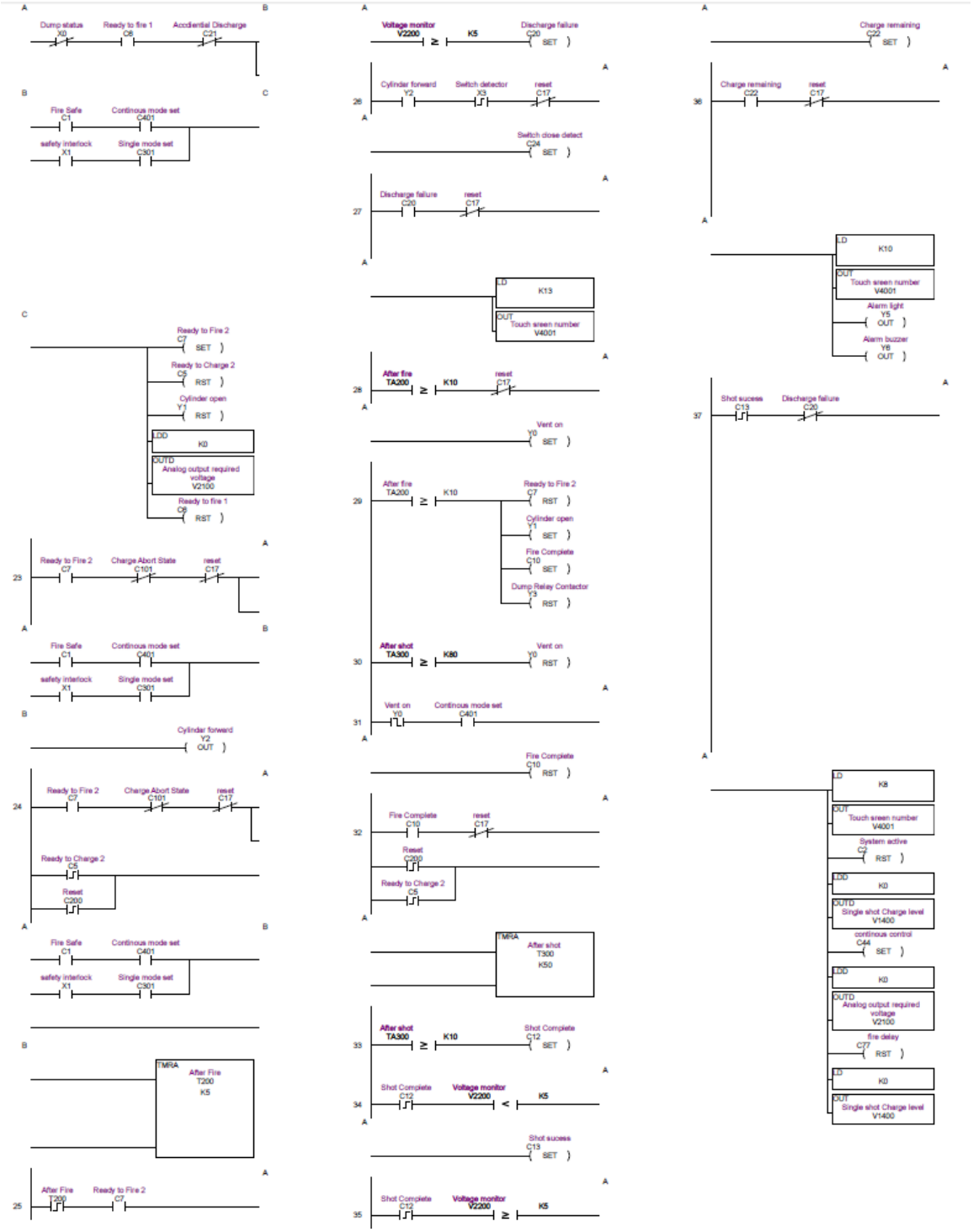
Dump status X0
Ready to fire 1 C6
Accidential Discharge C21
Fire Safe C1
Continous mode set C401
safety interlock X1
Single mode set C301
Ready to Fire 2 C7 SET
Ready to Charge 2 C5 RST
Cylinder open Y1 RST
LDD K0
OUTD Analog output required voltage V2100
Ready to fire 1 C6 RST
23
Ready to Fire 2 C7
Charge Abort State C101
reset C17
Cylinder forward Y2 OUT
24
TMRA After Fire T200 K5
25
After Fire T200
Ready to Fire 2 C7
Voltage monitor V2200 ≥ K5
Discharge failure C20 SET
26
Cylinder forward Y2
Switch detector X3
reset C17
Switch close detect C24 SET
27
Discharge failure C20
reset C17
LD K13
OUT Touch sreen number V4001
28
After fire TA200 ≥ K10
reset C17
Vent on Y0 SET
29
After fire TA200 ≥ K10
Ready to Fire 2 C7 RST
Cylinder open Y1 SET
Fire Complete C10 SET
Dump Relay Contactor Y3 RST
30
After shot TA300 ≥ K80
Vent on Y0 RST
31
Vent on Y0
Continous mode set C401
Fire Complete C10 RST
32
Fire Complete C10
reset C17
Reset C200
Ready to Charge 2 C5
TMRA After shot T300 K50
33
After shot TA300 ≥ K10
Shot Complete C12 SET
34
Shot Complete C12
Voltage monitor V2200 < K5
Shot sucess C13 SET
35
Shot Complete C12
Voltage monitor V2200 ≥ K5
Charge remaining C22 SET
36
Charge remaining C22
reset C17
LD K10
OUT Touch sreen number V4001
Alarm light Y5 OUT
Alarm buzzer Y6 OUT
37
Shot sucess C13
Discharge failure C20
LD K8
OUT Touch sreen number V4001
System active C2 RST
LDD K0
OUTD Single shot Charge level V1400
continous control C44 SET
LDD K0
OUTD Analog output required voltage V2100
fire delay C77 RST
LD K0
OUT Single shot Charge level V1400

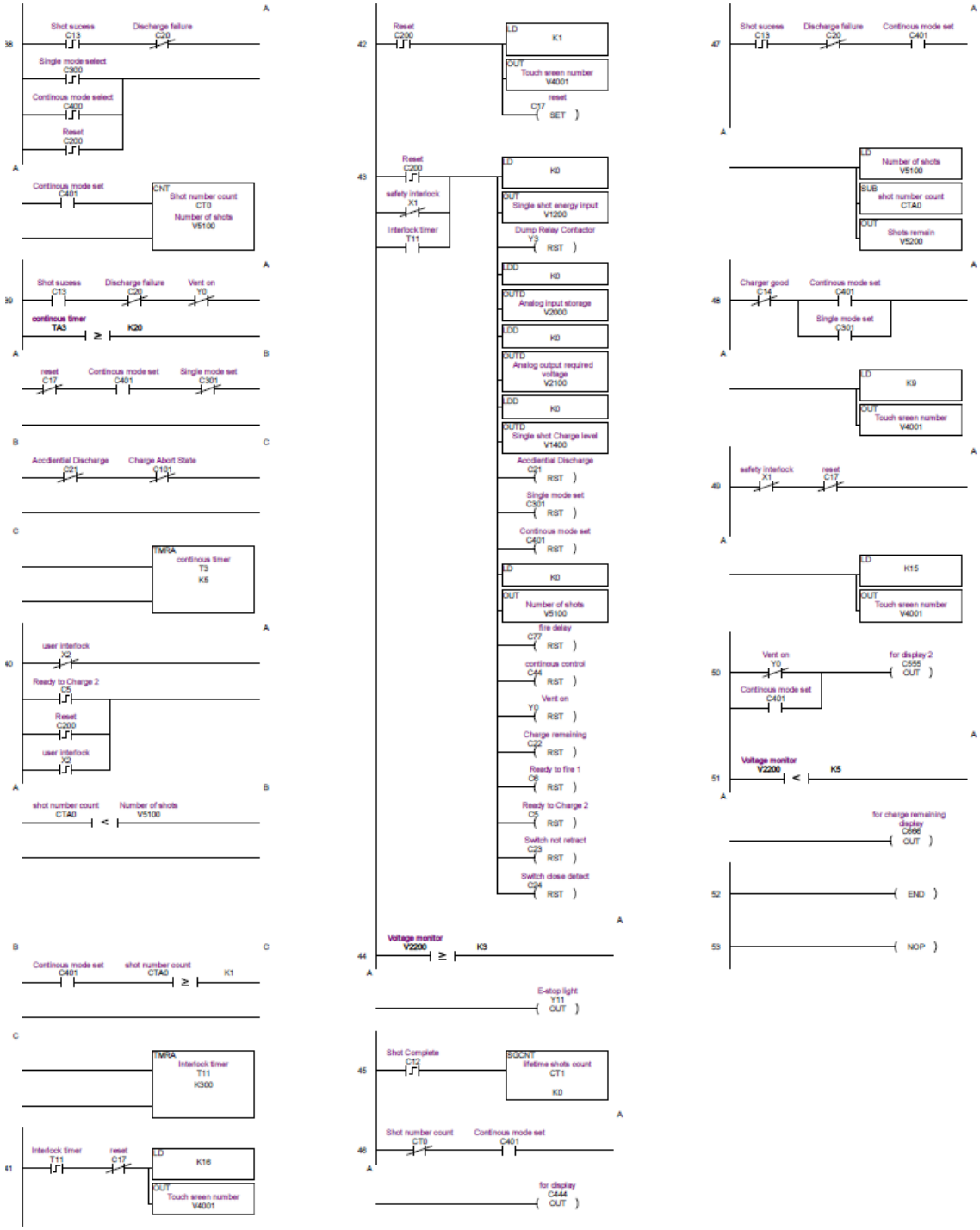
38
Shot sucess C13
Discharge failure C20
Single mode select C300
Continous mode select C400
Reset C200
Continous mode set C401
CNT Shot number count CT0 Number of shots V5100
39
Shot sucess C13
Discharge failure C20
Vent on Y0
continous timer TA3 ≥ K20
reset C17
Continous mode set C401
Single mode set C301
Accidential Discharge C21
Charge Abort State C101
TMRA continous timer T3 K5
40
user interlock X2
Ready to Charge 2 C5
Reset C200
user interlock X2
shot number count CTA0 < Number of shots V5100
Continous mode set C401
shot number count CTA0 ≥ K1
TMRA Interlock timer T11 K300
41
Interlock timer T11
reset C17
LD K16
OUT Touch sreen number V4001
42
Reset C200
LD K1
OUT Touch sreen number V4001
reset C17 SET
43
Reset C200
safety interlock X1
Interlock timer T11
LD K0
OUT Single shot energy input V1200
Dump Relay Contactor Y3 RST
LDD K0
OUTD Analog input storage V2000
LDD K0
OUTD Analog output required voltage V2100
LDD K0
OUTD Single shot Charge level V1400
Accidential Discharge C21 RST
Single mode set C301 RST
Continous mode set C401 RST
LD K0
OUT Number of shots V5100
fire delay C77 RST
continous control C44 RST
Vent on Y0 RST
Charge remaining C22 RST
Ready to fire 1 C8 RST
Ready to Charge 2 C5 RST
Switch not retract C23 RST
Switch close detect C24 RST
44
Voltage monitor V2200 ≥ K3
E-stop light Y11 OUT
45
Shot Complete C12
SUCNT lifetime shots count CT1 K0
46
Shot number count CT0
Continous mode set C401
for display C444 OUT
47
Shot sucess C13
Discharge failure C20
Continous mode set C401
LD Number of shots V5100
SUB shot number count CTA0
OUT Shots remain V5200
48
Charger good C14
Continous mode set C401
Single mode set C301
LD K9
OUT Touch sreen number V4001
49
safety interlock X1
reset C17
LD K15
OUT Touch sreen number V4001
50
Vent on Y0
Continous mode set C401
for display 2 C555 OUT
51
Voltage monitor V2200 < K5
for charge remaining display C666 OUT
52
END
53
NOP

Appendix D: The voltage and current traces of the system constructed and CB2

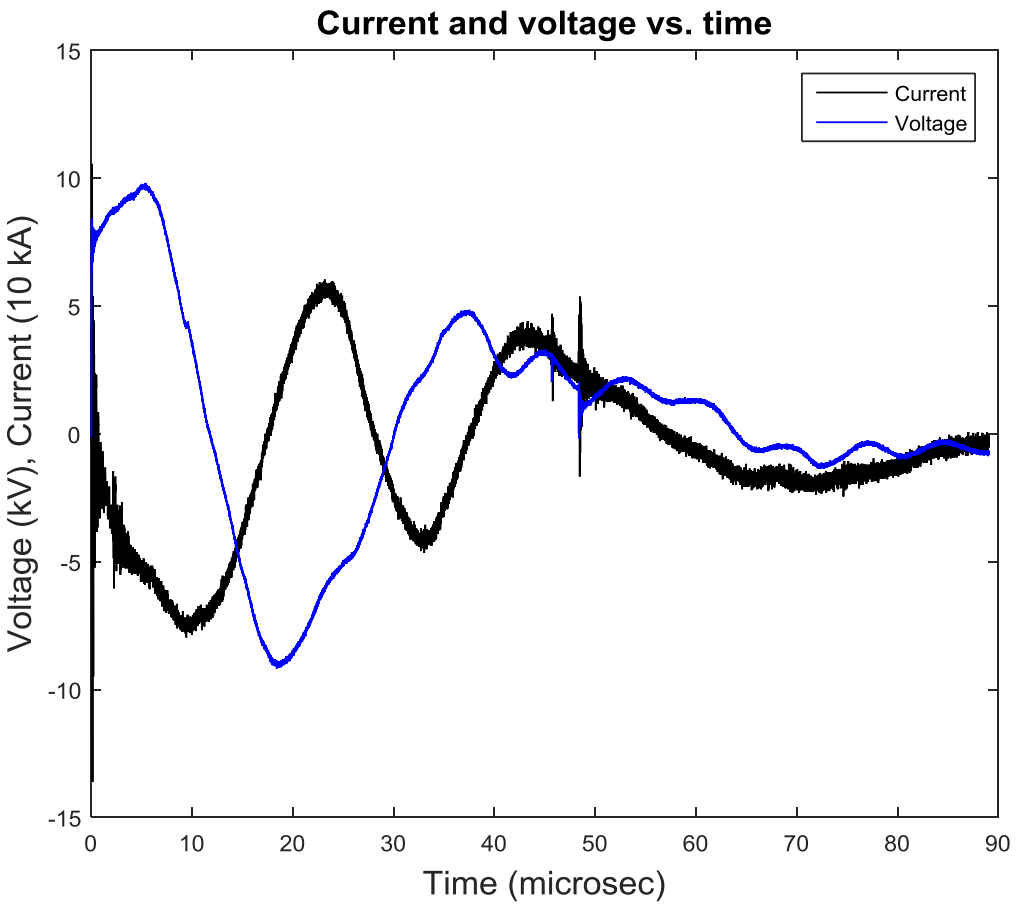

Fig. 29. Current and voltage trace of the system constructed when vaporizing foil with input energy of 2.6 kJ

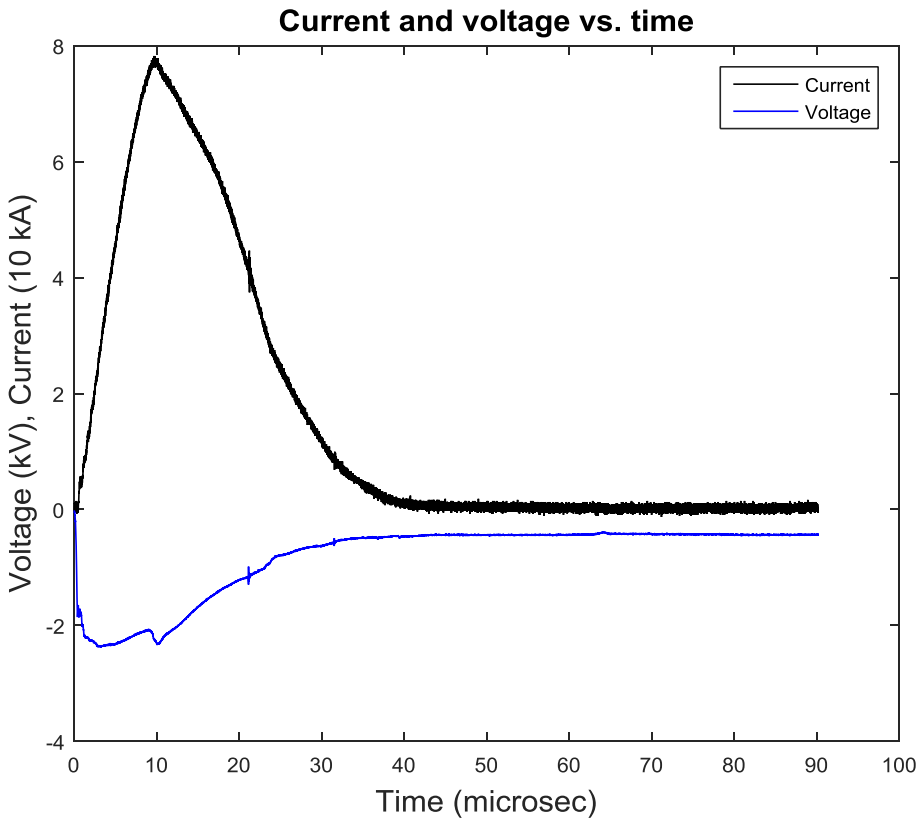

Fig. 30. Current and voltage trace of CB2 when vaporizing foil with input energy of 2.6 kJ